To the Graduate Council:

I am submitting herewith a thesis written by Marvis Kelly White entitled "The Effect of Environment on Thermal Cycling Damage in Boron-Aluminum Composites." I recommend that it be accepted in partial fulfillment of the requirements for the degree of Master of Science, with a major in Engineering Science.

Maurice A. Wright, Major Professor

We have read this thesis
and recommend its acceptance:

Walter Frost

Neil Loeffler

Accepted for the Council:

Vice Chancellor
Graduate Studies and Research

THE EFFECT OF ENVIRONMENT ON THERMAL CYCLING DAMAGE IN BORON-ALUMINUM COMPOSITES

A Thesis

Presented for the

Master of Science

Degree

The University of Tennessee, Knoxville

Marvis Kelly White

August 1976

1288112

ACKNOWLEDGEMENTS

The author wishes to express his sincere appreciation to Dr. M. A. Wright, Professor of Metallurgical Engineering at The University of Tennessee Space Institute, for his counsel, instruction, and encouragement throughout the course of this study and investigation.

The author is grateful to his colleagues of The University of Tennessee Space Institute Materials Laboratory for their cooperation, help, and discussion throughout this research. He especially wishes to thank E. Flowers for the original design and construction of the cycling furnace, D. Welch for the use of his computer program to reduce fiber data, and J. Jollay for his assistance in the lab.

The author would also like to thank Dr. C. H. Weaver, Dean of The University of Tennessee Space Institute, and the Department of the Navy, Washington, D. C., for the opportunity to conduct this investigation.

ABSTRACT

Boron-aluminum composites having 6061, 2024, and 1100 alloy matrices were subjected to 6,000 thermal cycles between ambient temperature and 425°C in argon and in air. Both longitudinally and transversely oriented specimens were used. Cycling in argon was performed using periods of six and twelve minutes per cycle. The cyclic period used in air was twelve minutes per cycle. The strength, stiffness, and Poisson's ratio properties were measured after cycling and compared to the same properties in the as-fabricated condition. Also, the strengths of fibers extracted from both cycled and uncycled materials were measured and compared. Metallographic observations and density tests were also conducted.

Little physical damage, as evidenced by surface roughening and cracking, was observed in the materials cycled in the inert gas. However, relatively severe damage occurred in those specimens cycled in laboratory air. Extensive surface roughening and cracking was observed. A decrease in density from that of the as-received material was also found. Tensile strength degradations greater than 50% were measured parallel to the fiber axis, while transverse strength reductions of as much as 77% were observed. Fibers extracted from specimens cycled in argon showed

little or no strength decrease while the fibers extracted from air-cycled specimens had large strength reductions.

The observations of increased thermal cycling damage in air compared to argon were explained on the basis of thermal corrosion fatigue damage to the matrix and reaction of the fibers with the matrix and with the air.

The stresses and strains generated in a composite during thermal cycling were calculated. Their contribution to the damage sustained by the material was evaluated.

TABLE OF CONTENTS

CHAPTER		PAGE
I.	INTRODUCTION	1
II.	THERMAL DAMAGE MECHANISMS	4
	Thermal Stresses and Strains	4
	Thermal Fatigue and Cyclic Creep	10
	Corrosion Fatigue	14
	Chemical Reaction	20
	Interphase reaction	20
	Environmental reaction	22
III.	EXPERIMENTAL PROCEDURES	25
	Test Material	25
	Thermal Cycling Tests	25
	Thermal Cycling Apparatus	26
	Mechanical Property Measurements	28
	Composite testing	28
	Fiber testing	29
	Physical Property Determination	30
	Physical measurements	30
	Metallographic observations	31
IV.	EXPERIMENTAL RESULTS	33
	Composite Mechanical Properties	33
	Fiber Strengths	35
	Composite Density	36
	Physical and Metallographic Observations	38

CHAPTER PAGE

V. DISCUSSION 41
Computed Thermal Stresses and Strains. 41
Composite Degradation. 45
Damage Mechanisms. 47
Matrix 47
Fibers and interface 50
VI. CONCLUSIONS. 52
VII. RECOMMENDATIONS. 54
BIBLIOGRAPHY 55
APPENDIX 61
VITA 92

LIST OF TABLES

TABLE PAGE

1. Measured Mechanical Properties of 6061 Matrix B-Al Composite 62
2. Measured Mechanical Properties of 2024 Matrix B-Al Composite 63
3. Measured Mechanical Properties of 1100 Matrix B-Al Composite 64
4. Experimental Data for Extracted 2 Inch Long Boron Fibers 65
5. Density Measurements of As-Received and Thermally Cycled B-Al. 66

LIST OF FIGURES

FIGURE		PAGE
1.	The Sub-surface of a Boron-Aluminum Specimen After 6,000 Cycles in Air	67
2.	An Apparent Oxide Film at the Interface of As-Received Boron-Aluminum.	68
3.	A Boron Fiber Covered with Reaction Products.	69
4.	The Speroidazation of a Thermally Cycled Boron-Aluminum Surface.	70
5.	A Diagram of the Controlled Atmosphere Thermal Cycling Furnace	71
6.	The Specimen Temperature During Thermal Cycling, 6 Minutes/Cycle	72
7.	The Specimen Temperature During Thermal Cycling, 12 Minutes/Cycle.	73
8.	An Instrumented Composite Specimen Gripped in the Tensile Machine	74
9.	A Typical Fracture Surface of 6061 Aluminum-Boron	75
10.	A Typical Fracture Surface of 2024 Aluminum-Boron	76
11.	A Typical Fracture Surface of 1100 Aluminum-Boron	77
12.	A Micrograph Showing the Poor Consolidation of the 1100 Aluminum-Boron	78

FIGURE PAGE

13. The Surface of 6061 Aluminum-Boron Thermally Cycled in Argon, 12 Minutes/Cycle 79

14. The Surface of 6061 Aluminum-Boron Thermally Cycled in Air, 12 Minutes/Cycle 80

15. The Surface of 2024 Aluminum-Boron Thermally Cycled in Argon, 12 Minutes/Cycle 81

16. The Surface of 2024 Aluminum-Boron Thermally Cycled in Air, 12 Minutes/Cycle 82

17. The Surface of 1100 Aluminum-Boron Thermally Cycled in Argon, 12 Minutes/Cycle 83

18. The Surface of 1100 Aluminum-Boron Thermally Cycled in Air, 12 Minutes/Cycle 84

19. A Flow-Chart for the Computation of Composite Thermal Stresses and Strains. 85

20. The Matrix Stress in Thermally Cycled 2024 Aluminum-Boron, 12 Minutes/Cycle 86

21. The Matrix Stress-Strain Curve During Thermal Cycling of 2024 Aluminum-Boron, 12 Minutes/Cycle. 87

22. The Creep Strain During Thermal Cycling of 2024 Aluminum-Boron, 12 Minutes/Cycle 88

23. The Fiber Stress During Thermal Cycling of 2024 Aluminum-Boron, 12 Minutes/Cycle 89

FIGURE PAGE

24. The Matrix Stress During Thermal Cycling of 2024 Aluminum-Boron, 6 Minutes/Cycle. 90

25. The Matrix Stress-Strain Curve During Thermal Cycling of 2024 Aluminum-Boron, 6 Minutes/Cycle 91

CHAPTER I

INTRODUCTION

The high specific strength and modulus properties of fiberous composite materials have resulted in much interest in their use for applications requiring high strength at low weight, particularly in the design of aerospace structures. Extensive effort has been put forth in the last decade toward development of these materials, improvement of fabrication methods, and understanding their behavior. This research has been directed toward composites in general, and toward individual composite systems.

This investigation concerns itself with the behavior of a particular metal matrix composite, boron-aluminum, subjected to cyclic temperature variations in the presence of argon and air environments. Its purpose was to determine the effects of these environments on the material's physical and mechanical properties and to attempt to define the mechanisms responsible for these effects.

The elevated temperature behavior of metal matrix composites is of great importance since they have their principal utility in high temperature applications. All of these materials have been shown to be adversely affected in

varying degrees by either static [1, 2][1] or cyclic [3, 4] elevated temperatures applications, often resulting in very substantial reductions in mechanical properties and in service life. Among the effects experienced are dimensional changes such as bending or twisting, surface roughening and cracking, internal void formation, reactions of the phases with each other or with the environment, matrix delamination, fiber-matrix interface disruption, and even fiber breakage. These, either separately or in combination, decrease the tensile strength and modulus, the Poisson's ratios and failure strain, and reduce the shear strength [4] and the fracture toughness [4].

A number of mechanisms such as chemical reaction, thermal fatigue, stress corrosion cracking, corrosion fatigue, hydrogen embrittlement, creep, precipitate particle segregation, grain coarsening, and others may contribute to the production of the detrimental effects of temperature on metal matrix composites. Their operation is often very complex due to the heterogeneous, anisotropic nature of the material, and to the fact that very often more than one mechanism function concurrently, either independently or conjointly.

In this investigation specimens of three aluminum alloys (6061, 2024, and 1100) reinforced with boron fibers

---

[1]Numbers in brackets refer to similarly numbered references in the bibliography.

were thermally cycled in both air and in a relatively inert atmosphere, argon, between room temperature and 425°C.

An increase in thermal cycling damage in air compared to argon was observed. This was explained on the basis of thermal corrosion fatigue damage to the matrix and reaction of the fibers with the matrix and with the air.

Calculations of the stresses and strains generated in a composite during thermal cycling were made. The results were used to determine whether the stress, the time independent plastic strain, or the creep strain was the primary source of damage.

CHAPTER II

THERMAL DAMAGE MECHANISMS

In this chapter the mechanisms that may be involved in producing detrimental thermal effects in fiber-reinforced metal matrix composites are discussed as well as the effects themselves.

Before discussing the actual mechanisms, however, it is first necessary to consider two of the key quantities involved in their action, thermal stresses and strains.

Thermal Stresses and Strains

In metal matrix composites having appreciably different thermal expansion coefficients between the component phases, large thermal stresses may be generated due to changes in temperature. Such stresses are generated during the service life of composites subjected to varying temperatures and are the driving forces behind such damage mechanisms as thermal fatigue, corrosion fatigue, and creep, as will be discussed later.

Residual stresses are produced in cooling from fabrication temperatures, as reported by Ebert and Wright [5] for boron-aluminum. The material is originally stress free at the fabrication temperature, approximately 500°C for B-Al. When the temperature is decreased, the longitudinal contraction of the matrix is constrained by the

fibers. This causes a longitudinal tensile stress in the matrix and a balancing compressive stress in the fibers. Shear stresses and lateral stresses as a result of Poisson's effects are also generated.

That this stress is sufficiently large to produce yielding in boron-aluminum may be shown by a macroanalysis of the elastic stresses, as performed by Wills [6] and Garmong [7]. Assuming that no external forces are applied, the stress equilibrium relation for the composite is given by the familiar rule of mixtures,

$$\sigma_f V_f + \sigma_m V_m = \sigma_c = 0 \qquad (1)$$

or

$$\sigma_f V_f = \sigma_m (1-V_f) \ , \qquad (2)$$

where

σ_f , σ_m , σ_c = fiber, matrix, and composite stresses ;

V_f , V_m = fiber and matrix volume fractions .

The method of virtual displacements [8] defines the strain continuity condition. The unconstrained thermal strains of the fibers and matrix due to a temperature change, dT, are $\alpha_f dT$ and $\alpha_m dT$, respectively, where α is the coefficient of thermal expansion. Assuming perfect bonding in the composite so that no slip occurs between the components, the fiber and matrix strains must be equal. Therefore,

$$\int_{T_1}^{T_2} \alpha_m dT + \varepsilon_m = \int_{T_1}^{T_2} \alpha_f dT + \varepsilon_f \ , \tag{3}$$

where ε is the mechanical strain due to stresses produced by the constraint of the other phase. By substituting Eq. (3) into Eq. (2) and using the constitutive relation, $\sigma = E\varepsilon$, the elastic stress in the matrix is given by

$$\sigma_m = \frac{E_m E_f V_f \int_{T_1}^{T_2} (\alpha_f - \alpha_m) dT}{E_f V_f - (1 - V_f) E_m} \tag{4}$$

or

$$\sigma_m = \frac{E_m E_f V_f (\alpha_f - \alpha_m) \Delta T}{E_f V_f - (1 - V_f) E_m} \ , \tag{5}$$

if the expansion coefficients are assumed constant.

Typical property values for boron-aluminum are:

$$E_m = 10 \times 10^6 \text{ psi} \ ,$$

$$E_f = 60 \times 10^6 \text{ psi} \ ,$$

$$\alpha_f = 4.9 \times 10^{-6}/°C \ ,$$

$$\alpha_m = 24 \times 10^{-6}/°C \ .$$

Using these values the elastic stress produced in the matrix upon cooling from a fabrication temperature of 500°C to room temperature would be about 77 ksi for 50% B-Al. This value

is well in excess of even the ultimate strength of aluminum. It is therefore evident from this sample calculation that temperature variations can produce large thermal stresses in a composite of sufficient magnitude to cause plastic deformation.

The total matrix strain, including elastic and inelastic components, for a one-dimensional composite having fibers considered to be infinitely stiff relative to the matrix would be [9]

$$\varepsilon_m = (\bar{\alpha}_f - \bar{\alpha}_m)\Delta T \ , \qquad (6)$$

where $\bar{\alpha}$ are the average coefficients of thermal expansion over the temperature range, ΔT. It may be seen that, as required for strain continuity, the mechanical strain produced in the composite is equal to the difference between the unconstrained thermal strains of its components.

In order to evaluate the actual stresses and the extent of the plastic flow which is to be expected due to a change in temperature, an extension of the analysis is required to include both time independent plastic deformation and time dependent plastic deformation, that is, creep. While creep effects in aluminum are small near room temperature, they would be expected to be very significant at combined high temperature and high stress.

Such an analysis is provided by Garmong [7]. The total mechanical strain of either component of the composite

is given by

$$\varepsilon = \varepsilon_e + \varepsilon_p + \varepsilon_c \ , \tag{7}$$

where

ε_e = elastic strain ,

ε_p = time independent plastic strain ,

ε_c = creep strain .

Considering only a one-dimensional state of stress and strain, the elastic component of Eq. (7) is given for either phase by

$$\varepsilon_e = \frac{\sigma}{E} \ . \tag{8}$$

Since the fibers may be assumed to always remain elastic, then

$$\varepsilon_f = (\varepsilon_e)_f \ . \tag{9}$$

The matrix plastic strain term may be provided by the Ludwick relation between stress and strain after yielding:

$$\sigma_m = \sigma_o + K_*[(\varepsilon_m)_p]^n \ , \tag{10}$$

where

σ_o = yield stress ,

K_* , n = constants .

Solving for strain,

$$(\varepsilon_m)_p = \pm \left[\frac{(\sigma_m - \sigma_o)}{K_*} \right]^{\frac{1}{n}} . \qquad (11)$$

The Dorn equation is employed for steady-state creep:

$$(\dot{\varepsilon}_m)_c = A\left(\frac{|\sigma_m|}{G} \right)^S \frac{Gb}{kT} D_o e^{-Q/RT} , \qquad (12)$$

where

G = shear modulus ,

Q = creep activation energy

$\simeq$ self-diffusion activation energy ,

b = Burger's vector ,

k = Boltzmann's constant ,

R = gas constant ,

A, S, D_o = constants .

Integrating over the temperature range of interest:

$$(\varepsilon_m)_c = \int_{T_1}^{T_2} (\dot{\varepsilon}_m)_c \frac{dt}{dT} dT$$

$$= \int_{T_1}^{T_2} A\left(\frac{|\sigma_m|}{G} \right)^S \frac{Gb}{kT} D_o e^{-Q/RT} \left(\frac{dt}{dT}\right) dT . \qquad (13)$$

By summing these strain components, substituting into Eq. (3) and eliminating σ_f by the use of Eq. (2), a single equation is obtained for the matrix stress, σ_m , as

$$\int_{T_1}^{T_2} (\alpha_m - \alpha_f) dT = \frac{\sigma_a - \sigma_m V_m}{V_f E_f} - \left\{ \frac{\sigma_m}{E_m} \pm \left[\frac{\sigma_m - \sigma_o}{K_*} \right]^{\frac{1}{n}} \right.$$

$$\left. \pm \int_{T_1}^{T_2} A \left(\frac{|\sigma_m|}{G} \right)^S \frac{Gb}{kT} D_o e^{-Q/RT} \left(\frac{dt}{dT}\right) dT \right\} , \qquad (14)$$

where σ_a is the applied stress and $\frac{dt}{dT}$ is the inverse of the heating rate.

This equation may be easily solved only by numerical methods. Results of a computer program written for this purpose are presented and discussed in Chapter V.

Thermal Fatigue and Cyclic Creep

These two subjects cannot be separated in a discussion of composite thermal cycling at high temperatures since they occur together and are interrelated.

Thermal fatigue, considered as a distinct mechanism, is herein restricted to signify the direct fatigue damage, in the absence of environment effects, produced in composites by the cyclic application of thermal stresses generated by the difference in expansion coefficients of the phases.

The term is sometimes used in the literature, however, to refer to the action of thermal stresses in any material, isotropic homogeneous or otherwise, induced in whatever manner (for example, by external restraint, non-uniform heating of complex shapes, or internal transformations involving volume changes). A thorough review of this type of thermal fatigue is given by Taira [10]. Also, for composites, the term is often used to indicate any and all mechanisms involved in producing detrimental effects by thermal cycling, such as creep, chemical reaction, corrosion fatigue, and so forth.

Matrix damage due to combined thermal fatigue and creep is, for a given material, a function of stress, temperature, and time. Cyclic stresses, whether above or below the gross matrix yield stress, produce reversed plastic strains which initiate fatigue cracks and cause them to propagate [11]. These stresses may be either applied or thermal. The cracks initiate primarily at the surface, at the fiber-matrix interface, and at inclusions in the matrix. Figure 1 of the appendix[2] shows the sub-surface of a 2024 Al-B specimen thermally cycled in air.

Wright [12] reported the results of varying the thermal cyclic period applied to several metal matrix composites. It was found that increasing damage became apparent as the frequency decreased, indicating that the

---

[2]All figures appear in the appendix.

time that the materials remained at elevated temperatures was of key importance.

The effect of the cyclic temperature limits was demonstrated by the same author [4]. Boron-aluminum materials were subjected to 6,000 cyclic variations in air between ambient and upper limits of 315, 365, and 425°C. The extent of matrix degradation was shown to increase substantially, for a given cyclic period, as the upper temperature limit was increased. Part of this result was possibly due to the increased rate of temperature change working in conjunction with environmental effects. At sufficiently elevated temperatures, large but relatively slow temperature changes would not be expected to create large stresses due to the relaxing effect of large creep deformations.

Creep mainly involves the movement of dislocations [11]. It is a diffusion and stress controlled phenomenon and, therefore, is primarily affected by temperature, stress, time, and material ductility. According to Eq. (12), the creep rate is proportional to the temperature and also the variation of the creep activation energy with temperature. This activation energy is approximately the same as that for self-diffusion. It increases with temperature, tending to decrease the creep rate [13].

As also seen from Eq. (12), the creep rate is proportional to a positive power of the stress, about 4.4 for aluminum. It is inversely proportional to a ductility

parameter. The ease of dislocation movements is influenced by crystallographic structure, grain size, and the presence of precipitate particles and inclusions.

The maximum possible thermal stress in the matrix is somewhat in excess of the yield stress as determined by the extent of work hardening and stress triaxiality. The greater the yield stress and work hardening, the greater the maximum stress and hence, the plastic strain. In thermal cycling B-Al composites in air, Shahanian [3], Wright [4], and others have found that the maximum matrix degradation occurs in aluminum alloys having the highest yield stress. For example, among the matrix alloys, 6061, 2024, and 1100, the 2024 aluminum was the most degraded.

An approximate relationship often used in predicting the life of a material subjected to mechanical fatigue is the Manson-Coffin law. This states that the number of cycles to failure is inversely proportional to a positive power of the plastic strain range or amplitude, that is,

$$N = \frac{D}{(\Delta\varepsilon_p)^z} = \frac{\ell n(1/(1-RA))}{(\Delta\varepsilon_p)^z} , \qquad (15)$$

where

N = number of cycles to failure ,

$\Delta\varepsilon_p$ = plastic strain per cycle ,

D = a ductility parameter ,

RA = fractional reduction in area
in a tensile test ,

z = empirical constant, usually between
1.5 and 2 .

According to Manson, this relation is valid for at least some thermal cycling experiments also. For a composite, N is expected to be the number of cycles required to reduce the load carrying capacity of the matrix to zero, that is, to make it ineffective.

Corrosion Fatigue

Corrosion fatigue is defined as the reduction of fatigue resistance due to the presence of a corrosive medium [14]. While often considered a special case of stress corrosion cracking (SCC), the two phenomena have distinctly different mechanisms of crack initiation and propagation and different material-environment interactions. Stress corrosion cracking for a given material requires the presence of very specific corrodents. However, corrosion fatigue will generally occur in any corrosive medium and, usually, at lower corrodent concentrations [15].

Most fatigue failures are probably, in fact, corrosion fatigue failures since they occur in some corrosive environment, if only air. Corrosion fatigue is perhaps the biggest, most complex problem in metals research and utilization today. This is because of the large number

of interacting variables involved, the fact that response to these variables is different in different stages of fatigue, and because of the inability to actually observe the processes that occur.

While the exact mechanisms of corrosion fatigue in aluminum and its alloys are as yet uncertain, the phenomenological aspects are quite well known. The principal ones are listed here [16, 17, 18, 19].

1. Water vapor is the primary agent affecting the fatigue properties. Depending upon the alloy and various test variables, moisture can increase the rate of crack growth by a factor of ten or more. Dry oxygen and hydrogen have only a small effect at room temperature. The effect on pure Al is somewhat greater than on its alloys. Dry nitrogen and argon have essentially no effect. The effect of humid gases is predominantly determined by their water vapor content.

2. The fatigue crack growth rate varies with water vapor pressure. The rate is essentially unaffected until a threshold pressure is reached and then, usually within one order of magnitude change, increases rapidly with increasing pressure. This threshold or transition pressure has been found to increase with both increasing frequency and crack length.

3. An increase in test frequency results in a larger number of cycles to failure because of the lesser

amount of time for environmental interactions. At high stress intensity levels the actual time to failure is usually less. However, at low amplitudes, it is often larger due to increased endurance limit.

4. The magnitude of the environmental effect is greatest at low values of the stress intensity amplitude, K, corresponding to the shortest crack lengths. At high values of K approaching K_c , the environmental sensitivity decreases due to the predominating gross plasticity effects.

5. Thin sections are less environmentally sensitive. Wei [16] ascribes this to the increased stress-relieving effect of plastic deformation associated with a transition from a plane stress to a plane strain mode of fracture. According to the hydrogen embrittlement mechanism, to be discussed later, the environmentally produced stresses are believed to be generated by the pressure of evolved hydrogen in the matrix.

6. At a given K level, the fatigue crack growth rate increases with increasing temperature.

7. Distinct failure striations are produced in air but not in vacuum. Aggressive environments at low frequencies and amplitudes result in a change from normal ductile striations to brittle striations. These are flat, reflective facets exhibiting faint crack arrest markings.

The fatigue fracture process is normally separated into four phases [19]. Crack initiation, usually at surfaces, involves the formation and coarsening of slip bands until microcracks are produced. During stage I propagation these microcracks grow by shear along slip bands until the stress concentration increases the tensile component sufficiently to cause the crack to grow approximately perpendicular to the applied stress. This is stage II propagation. The last phase is rapid brittle fracture.

The relative effects of environment on crack initiation and propagation rates are not well agreed upon. Some investigators, such as Broom and Nicholson [20] and Grosskrentz [21], state that the effect of water vapor is greatest during the initiation and stage I propagation phases of fatigue. Wadsworth and Hutchings [22] and others contend that while initiation is relatively insensitive to environment, propagation is greatly accelerated. The difference between these observations is probably due to differences in alloy types, frequency, stress conditions, and other test variables.

Even less agreement is found on the mechanisms of fatigue crack growth and initiation in aluminum. Almost as many theories exist as do investigators. However, they may be grouped broadly into three classes: (1) gas adsorption, (2) hydrogen embrittlement, and (3) slip interaction with

surface oxide films. These will be briefly described in the following paragraphs.

The adsorption model, as advocated by Wadsworth and Hutchings [22] and others, considers that gas molecules flow into a newly formed portion of crack during tension, become adsorbed in a monolayer and prevent crack rewelding and reversed slip during compression. The dominant effect of water vapor as compared to other gas species was explained by the fact that it adsorbs on the surface to a greater extent.

The hydrogen embrittlement model may apply to either crack initiation or propagation, according to Bloom and Nicholson [20] and Wei [16]. Water vapor will react with newly formed surfaces, producing atomic hydrogen and aluminum oxide. The oxide covers the crack surface preventing rewelding while atomic hydrogen is believed to be driven into the region ahead of the crack, super-saturating the lattice and reducing its strength. Subsequent precipitation of molecular hydrogen produces voids ahead of the crack tip which coalesce during the next tensile half-cycle.

Interaction of dislocations with oxide films [23, 24] can also be applied to both initiation and propagation of cracks. It is also called the "oxide film model" or "wet film model." In it the ratio (Γ) of a surface oxide film modulus to the substrate modulus is believed to control

dislocation interaction. If $\Gamma > 1$, dislocations are repelled from the film, and if $\Gamma < 1$, they are attracted. It was found that while Γ in vacuum is about five, at laboratory air humidity, it is about 0.5. Thus, in humid air dislocations would be attracted to the film, resulting in crack initiation or growth, while in vacuum they would not.

Some inconsistencies exist in each of these models and no model as yet explains satisfactorily all observed phenomena of aluminum corrosion fatigue.

Finally, the effect of corrosion fatigue on B-Al composites has been demonstrated by Smith and Shahanian [25]. They mechanically fatigued longitudinal and transverse specimens of 40% 2024 Al-B under cyclic bending in vacuum at 10^{-7} torr, in water vapor at pressures up to 5 torr, and in ambient air. Transverse specimens bent in the thickness direction showed a factor of 10 decrease in fatigue life in water vapor compared to vacuum. The transverse specimens cycled in the width direction indicated a factor of 190 decrease in 2 torr water vapor compared to vacuum. The longitudinal specimens cycled in the thickness direction showed a factor of 90 reduction in number of cycles per amount of crack growth prior to the occurrence of shear splitting of the matrix parallel to the fibers. While it is not sure how results from this type of test would relate to those under cyclic tension, it is evident that a large

effect of moisture exists, possibly even greater than that of the aluminum alone.

Chemical Reaction

The next damage mechanism to be discussed is chemical reaction. This problem stems from two sources: (1) reaction of the composite phases with each other, and (2) their reaction with various environmental constituents.

Interphase reaction. Boron and aluminum are thermodynamically unstable while in contact with each other at elevated temperatures [26]. Aluminum diboride is the result of this reaction, which involves a 20% decrease in volume.

Aluminum oxide (Al_2O_3) was identified at the boron-aluminum interface in work at the Midwest Research Institute [5]. Klein and Metcalfe [26] also report the presence of this oxide film. Figure 2 shows a SEM photograph, taken during the present investigation, of what appears to be such a film in boron-aluminum in the as-fabricated condition.

The aluminum oxide layer is believed by the same authors to act as a reaction barrier between the fibers and the matrix [26]. So long as it remains intact the diffusion of atoms across the interface to react with the other phase is impeded. However, according to this hypothesis, if the film became locally disrupted by thermal fatigue processes, reaction would be able to proceed rapidly at these sites.

In order to reduce interphase diffusion some composites are provided with diffusion barriers such as carbide, oxide, or nitride coatings on the fibers.

During long time exposure to elevated temperatures of about 600°C, large scale diffusion and reaction occurs at the interface of B-Al composites reinforced with uncoated fibers [1]. According to Klein and Metcalfe [26], a layer of aluminum diboride is formed at the interface. A similar layer observed in the present work is shown in Figure 3. Metallographic examination of these layers by Klein and Metcalfe showed them to be extensively cracked, probably because of the volume change involved in their formation. They ascribed the reduction in strength of fibers covered with aluminum diboride to the stress concentrating effect of cracks present in this surface layer. This conclusion was supported by an experiment in which they removed the aluminum diboride from reacted fibers with red fuming nitric acid. It was found that the strengths returned to within 93% of their original value.

A small amount of interphase reaction has been reported to slightly increase the composite strength due to improved interfacial bond. However, continued reaction drastically reduces that strength by lowering the strength of both the boron fibers and of the interface across which loads must be transferred by shear.

Environmental reaction. The other reaction problem in boron-aluminum composites is with its environment. This is particularly true when they are exposed to elevated temperatures or thermal cycling. The discussion here will be restricted to reaction with normal atmospheric species such as oxygen, nitrogen, and water vapor.

Both aluminum and boron are reactive with oxygen and nitrogen at high temperature. That large scale reaction does not occur when B-Al composites are heated in air is due primarily to the fact that the molecular gases are unable to diffuse through the matrix. A surface film of aluminum oxide is formed on the matrix even at room temperature which serves as a barrier against further surface reaction. Nitrogen, which has a lower reactivity than does oxygen, will produce a nitride film on oxide-free aluminum at elevated temperature.

Water vapor in the air will react with fresh aluminum surfaces, as previously mentioned. This reaction forms aluminum oxide and atomic hydrogen [27]. While molecular hydrogen cannot diffuse through the aluminum, atomic hydrogen can readily do so. Once in the metal, it has been proposed that the hydrogen causes hydrogen embrittlement or hydrogen blistering. The aluminum oxide formed at the surface during the reaction with water vapor would act to retard subsequent reaction.

Thermal cycling of a composite might be expected to result in greatly increased amounts of reaction with the atmosphere. This would occur if thermal fatigue breaks up the protective Al_2O_3 film and exposes new aluminum surfaces to the air. The reaction products could embrittle the surface and act as nucleation sites for the formation of fatigue cracks.

Another proposed method by which the matrix surface may be disrupted is called spheroidazation [28]. The high surface tension of the surface oxide film tends to cause the surface material to ball-up at high temperatures when the aluminum is extremely soft. An example of matrix surface ball-up is shown in Figure 4.

Once sufficient matrix cracking is produced to expose the fibers to the air, their oxidation becomes possible. According to Galasso [29], the room temperature strength of boron fibers heated in air for an hour is not drastically reduced unless they are heated over 500°C. Above 500°C the boron oxide formed becomes fluid and flows, allowing continued rapid oxidation. The strength is reduced to zero by heating to 600°C for an hour in air. Below 500°C the oxide layer serves to protect against further oxidation. The strengths of those heated in air below 500°C were about the same as for fibers heated in purified argon to the same temperatures.

Boron fibers contained in an aluminum matrix but exposed to the air by matrix cracking might be expected to

show greater amounts of oxidation than do fibers not in a composite. The thermal stresses and strains would be expected to produce cracks in the aluminum diboride and boron oxide films where continued localized oxidation could occur leading to stress concentrations and lower fiber and composite strengths.

CHAPTER III

EXPERIMENTAL PROCEDURES

Test Material

The composite materials used in this investigation consisted of three types of aluminum alloy matrix reinforced with boron filaments. The alloys were 6061, 2024, and 1100 aluminum. The boron filaments were 5.8 mil in diameter with the exception of the 6061 alloy material which contained 4.0 mil fibers. This 4-mil fiber composite material was received ready-cut from the NASA Marshall Space Flight Center, Alabama. The remainder of the materials was obtained from the Amercom Corporation in the form of sheet panels fabricated by the hot press diffusion bonding process.

The composite panels were cut by electric discharge machining (EDM) into specimens 6 inches long by 0.5 inch wide, the same size as the 4-mil fiber specimens. The thickness of all the materials was about 0.05 inch. Half of the specimens were cut longitudinal to the filaments and the other half transverse to the filaments.

Thermal Cycling Tests

Three groups of B-Al composite specimens were thermally cycled. These consisted of 6 and 12 minutes/cycle tests in argon and a 12 minutes/cycle test in air. Each group was comprised of 12 specimens, two longitudinal and

two transverse of each of the three material types, with the exception of the group cycled in air. Only one transverse specimen of the 2024 and 1100 matrix materials was available. Each group of specimens was subjected to a cyclic temperature variation between a maximum temperature of 425°C and a minimum as near room temperature as could be obtained.

Tests were performed at the two cyclic rates of 6 and 12 minutes/cycle in argon to study the effect of heating rate and time at temperature. Such tests in air have been made previously at The University of Tennessee Space Institute.

Thermal Cycling Apparatus

The principal piece of equipment used in this investigation for the thermal cycling of composite specimens is diagramatically depicted in Figure 5. It was originally built and used as a furnace for the directional solidification of eutectic alloys and was modified by the author for this investigation.

It consisted of an electrical resistance heated cylindrical furnace, movable along its axis about which were positioned the specimens to be cycled. These specimens were mounted against the sides of a hexagonal stainless steel cooling block through which water flowed during the cooling part of the cycle. The cooling block and specimens were sealed in a Vycor glass tube which could be evacuated of air and back-filled with a gas. During the heating part of the

cycle, the furnace was lowered over the glass tube by a motor until its hot zone was positioned opposite the specimens. The entire cycling operation, including the furnace movement and the coolant flow control, was automatically activated by a timing circuit.

Power to the furnace was supplied by a solid-state power controller which worked in conjunction with a proportional temperature controller. The furnace temperature required to heat the specimens to a given maximum temperature was set on the temperature controller. It maintained this temperature by causing the power delivered to the furnace to vary within limits pre-set on the power controller.

The temperature of the specimens was measured by a chromel-alumel thermocouple positioned against the surface of one specimen, midway along its length. It was assumed that all of the specimens were at the same temperature. The temperature was indicated on a temperature pyrometer and recorded at intervals on a strip chart. Figures 6 and 7 show the temperature curves for the 6- and 12-minute cycles.

It was found that the flow of water through the cooling block was insufficient to reach the desired lower temperature limit in the time allotted. Therefore, a blower was used to circulate air around the glass tube to cool it and the specimens within. This allowed a low temperature of about 150°C for the 6-minute cycles and about 55 to 75°C for the 12-minute cycles.

The inert atmosphere thermal cycling was conducted by evacuating the air from the glass tube with a mechanical vacuum pump. After a pressure of 1 to 2 mm of mercury had been attained, the unit was backfilled with argon to a pressure of about 2.5 psig. The system was re-evacuated and backfilled at intervals to purge out possible contaminants.

During the cycling in air, the system configuration was kept the same as for argon cycling. The only change was that the gas inlet to the glass tube was open to the room air.

Mechanical Property Measurements

Composite testing. The tensile strengths, elastic moduli, and Poisson's ratios were determined from longitudinal and transverse specimens in both as-received condition and after thermal cycling. These tests were made with an Instron universal testing machine having a 10,000-pound capacity.

Aluminum grip tabs (0.5 x 1.5 inch) were glued to each end of the specimens with an epoxy adhesive to prevent crushing and premature failure of the test pieces in the jaws of the test machine. The specimen gage length was, therefore, 3 inches.

Half of the test specimens were instrumented with strain gages for the measurement of elastic moduli and Poisson's ratios. Four strain gages, one oriented

longitudinal to the specimen axis and one transverse on each side, were mounted on these specimens with Eastman 910 cement. The response of these gages was monitored either as a continuous trace on the strip chart of the test machine or as discrete readings on a BLH strain indicator. Figure 8 shows an instrumented test specimen mounted in the tensile machine.

The remaining specimens were tested in the tensile machine without strain gages; however, an extensometer was mounted on each of these specimens in order to produce a stress-strain curve from which the elastic modulus and the failure stress and strain could be determined. The primary information provided by these specimens was the failure stress since the extensometer response was not adequate to give good accuracy in the determination of the other properties.

Fiber testing. Boron fibers were extracted from cycled and uncycled specimens of each material type by dissolving away the matrix in a sodium hydroxide solution. Fifty fibers from each specimen were pulled in the testing machine and the failure loads recorded.

Based on these loads and the measured fiber diameters, a statistical analysis was performed with the computer to determine the mean strength of each fiber set and the parameters of the Weibull statistical distribution

to which the fiber strengths conform [6]. From the Weibull parameters the mean of the distribution and the coefficient of variation were computed. The effects of the thermal cycling on the fiber strength could be evaluated from these results.

Physical Property Determination

Physical measurements. Prior to thermal cycling or mechanical testing, the width and thickness dimensions of each specimen were measured with a micrometer. These dimensions, taken as the average of three readings along the specimen length, gave the cross-sectional area needed for the determination of stresses and moduli. Measurement of dimensions after thermal cycling showed no significant change.

The volume fraction of fibers in each type of material was determined by counting under the microscope the number of fibers in the cross section. Knowing the mean fiber diameter, the total area of fibers in the section was calculated. Dividing by the total area of the cross section gave the area fraction of fibers equal to the volume fraction.

Measurements of specimen density before and after thermal cycling were done for each material in order to check for the formation of internal voids and cracks due to thermal cycling or of reaction products of different density

from the original material. These measurements were done by the Archimedes method which consists of weighing the sample first in air and then submerged in a liquid of known specific gravity. The liquid used was methyl ethyl ketone (MEK) which thoroughly wet the material. The analytical balance used to make the measurements could be read to an accuracy of ±0.001 gram. The density was calculated using the formula

$$\rho = \frac{A\rho_{MEK}}{A+H-F} , \tag{16}$$

where

A = weight of sample in air ,

H = weight of sample holder in liquid ,

F = weight of sample holder and sample in liquid ,

ρ_{MEK} = density of MEK = 0.802 gm/cm^3 .

Metallographic observations. Qualitative studies were made of specimen surface roughness and cracking before and after thermal cycling using a low magnification optical microscope. Photographs of the surfaces were taken through the microscope using oblique lighting. Observations and photographs were also made of the fracture morphology of each type and orientation of composite specimen in the

as-received and thermally cycled conditions. Sections of selected specimens were ground and polished for observation in the microscope.

Both an optical microscope and a scanning electron microscope were used in these studies, the purpose of which was to ascertain visible evidences of the degrading effects of thermal cycling which would yield information on the mechanisms involved.

CHAPTER IV

EXPERIMENTAL RESULTS

Composite Mechanical Properties

The measured ultimate tensile strengths, elastic moduli, and Poisson's ratios of the as-received and cycled 6061, 2024, and 1100 matrix boron-aluminum materials are compared in Tables 1, 2, and 3 of the appendix.[3]

In Table 1 it may be seen that the strengths of the 6061 aluminum 4-mil boron longitudinal specimens thermally cycled in argon did not decrease below that of the as-received material. A 65% decrease in strength, however, was noted for those cycled in air. For the 6061 transverse specimens cycled in argon, a 9% decline in strength was measured at 6 minutes/cycle and 23% at 12 minutes/cycle. No transverse 6061 Al-B specimens were thermally cycled in air as part of this investigation. But results of other work at The University of Tennessee Space Institute indicate an average 31% decline in the transverse strength after 6,000 cycles at 12 minutes/cycle [30].

The strength of 2024 aluminum reinforced with 5.8 mil boron fibers was also unchanged when cycled at either 6- or 12-minute periods, as is seen in Table 2. But when they were cycled in air at 12 minutes/cycle, a 61% decrease

[3]All tables appear in the appendix.

was found. A large decrease in transverse strength during argon gas thermal cycling was measured for the 2024 material. Part of this decrease may be attributable to annealing of the matrix rather than degradation. Since 2024 alloy is highly age hardenable and the specimens were not pre-annealed, it cannot be determined how much of the transverse strength loss was due to thermal cycling damage. A 5% greater strength loss was measured for the 12 minutes/cycle in air than for those in argon.

Similarly to the other materials, the 1100 matrix results, tabulated in Table 3, show little or no longitudinal strength degradation in argon, but a 44% decrease in air. The transverse strength dropped from 8 ksi in the as-received condition for both 6 and 12 minutes/cycle in the inert gas to 4 ksi at 12 minutes/cycle in air.

In comparing the three types of material it is seen that the 2024 was the strongest as-received and the 6061 was the weakest. The 6061 matrix material also showed the greatest longitudinal strength degradation in air. This was probably because of the inferior fibers it contained, as will be shown later by their lower as-received strengths and their large amount of longitudinal splitting. In addition to the fact that small diameter boron fibers are inherently weaker than larger ones, the 4-mil fibers in this 6061 material were of an older manufacture and contained many radial cracks as did all boron fibers prior to about 1970. The least strength loss was evidenced by the 1100 material.

Due to the amount of scatter in the modulus and Poisson's ratio data, it is not possible to determine from them any trends in the behavior of these properties when subjected to the various thermal cycling treatments.

Fiber Strengths

The results of the fiber strength tests described in the previous chapter are summarized in Table 4. The arithmetic, geometric, and Weibull mean strengths are given for each set of fibers. Also shown are the Weibull parameters, ω and σ_o, and the coefficient of variation, a measure of data scatter. The last column gives the percent change in Weibull mean fiber strength compared to as-received.

Little change in strength was obtained for the fibers extracted from argon atmosphere cycled specimens with the exception of the 2024 Al-B at 12 minutes/cycle. A 9% decrease from the as-received strength level was found for those fibers. In view of the fact that no corresponding decrease was seen in the longitudinal composite strength, improper procedure in extracting the fibers is suspected.

Quite large fiber strength degradations, on the other hand, were measured for those extracted from specimens thermally cycled in air. The decreases were 48, 23, and 18%, respectively, for the 6061, 2024, and 1100 matrix materials. Again, it is reasoned that the original inferior quality of

the 4-mil fibers may largely account for the greater amount of degradation they sustained.

Also, as indicated in Table 4, the variation in fiber strength for the 6061 and 2024 matrix composites increased during air cycling compared to that measured for as-received fibers. The greatest change is seen to be for the 2024 composite fibers. A smaller increase in strength variation occurred for those fibers cycled in argon at 12 minutes/cycle. The least change is seen in the 1100 material fiber scatter. These results are in agreement with observations of the composite specimens' failure modes to be discussed later. They also agree with the observation that early fiber breakage, audibly detected during loading of as-received composite specimens, was a minimum for 2024 and a maximum for 1100. Appreciable amounts of early fiber breakage, indicating a large strength variation, were noted for all specimens that had been cycled in air.

Composite Density

The influence of thermal cycling in argon and in air on the composite density is shown in Table 5. Despite the data scatter it is evident that an appreciably larger density change occurred during cycling in air than occurred in the inert environment. This indicates the formation of more internal voids in the air cycled materials than in those cycled in argon.

It may be seen that the largest apparent density change was in the 1100 material. This might at first seem suspect since the 1100 material was the least degraded according to the strength tests of the composite and the fibers and according to physical observation.

Two possible explanations exist. The first assumes that the apparent effect was real and was due to the inferior consolidation of the 1100 material. It may be that the thermal cycling opened up somewhat the original gaps between fibers and between the aluminum and the fibers to give a greater density change than occurred for the other two better consolidated materials.

The second possibility is that the measurements for the 2024 and 6061 specimens were erroneous due to the nature of the method. It should be pointed out that the word "density" is used here to mean gross density, that is, mass divided by gross volume. Porosity, which is the quantity of interest is

$$\text{Porosity} = \frac{\text{net density} - \text{gross density}}{\text{net density}} .$$

The net density is not known. However, providing it is constant, the change in porosity is indicated by the change in gross density. For correct results it is necessary that no penetration of the specimen by the fluid occurs. Some penetration did occur in the thermally cycled specimens due to the surface cracking. This would decrease the volume of

fluid displaced, resulting in a higher apparent density. The amount of error would be greatest for the 2024 and least for the 1100, since that was the order of cracking damage. A combination of these two possible effects is suspected.

It might be noted that if voids form as a result of localized transformations resulting in volume changes within a material, no change in the apparent density will be measured provided penetration of the fluid into the voids does not occur. If it does occur, an apparent increase in density will be measured.

Physical and Metallographic Observations

Observations of the fracture surfaces of longitudinal composite specimens revealed some information about the failure modes and the quality of the interfacial bond. No significant changes in the macroscopic fracture appearances were evident due to thermal cycling in either environment. As shown in Figure 9, the 6061 matrix specimens containing 4-mil fibers displayed a slightly jagged fracture surface, indicating a somewhat ductile failure. This was probably caused by deviation from perfect bonding, as evidenced by a small amount of fiber pullout. The 2024 material, however, showed a relatively flat fracture, as seen in Figure 10, and no fiber pullout, indicative of good consolidation and bonding. Figure 11 shows the extremely jagged fracture appearance of the 1100 matrix material due to a large amount of fiber pullout.

Poor consolidation of the material is evident from Figure 12.

The fracture surfaces on the transverse specimens were also viewed through a low power microscope. The 6061 material showed an extensive amount of fiber splitting due to its previously mentioned inferior quality while almost none occurred in the other materials. The 2024 transverse specimens failed by a mixture of separation in the matrix and at the interface. Transverse failure in the 1100 material was almost entirely at the interface.

Observation of the specimens' surface appearance before and after thermal cycling provided an indication of the amount of degradation. As viewed through a low power microscope, all of the cycled specimens displayed a greater amount of surface roughness than did the uncycled ones. However, the extent of this roughness was considerably greater for those that were thermally cycled in air. Figures 13 through 18 show surface photographs of each material type after 6,000 cycles in argon and in air at 12 minutes/cycle. It may be seen that the greatest difference is evident for the 2024 matrix composite and the least for the 1100 material. Little surface cracking was found for the argon cycled specimens, but a great deal for the air cycled ones.

The results of two studies with a scanning electron microscope proved inconclusive. The first consisted of examining the aluminum matrix fracture appearance to detect

differences that might be correlated with the amount of matrix degradation. It was suspected that the more damaged ones would show a more open, honeycomb-type fracture appearance due to the presence of reaction products. However, from the limited number of samples examined, it could not be determined that such was the case.

The purpose of the second SEM study was to compare the relative amounts of reaction product on extracted boron fibers. If fiber oxidation occurred in air, then more reaction material would be expected on the air cycled fibers. No conclusive trend, however, was apparent. While in some cases, the amount of reaction product did appear to increase with increased cyclic period and with exposure to air, in other cases the amount seemed random. It was concluded that quite a large number of fibers would have to be examined to positively determine correlations between visible fiber degradation and thermal cycling conditions or measured strength.

CHAPTER V

DISCUSSION

Computed Thermal Stresses and Strains

Using the analysis presented by Garmong [7] and previously discussed in Chapter II, a Fortran computer program was written to calculate the expected stresses and strains in a boron-aluminum composite during thermal cycling.

The matrix stress, σ_m , was evaluated for an assumed constant rate of cooling from the 500°C fabrication temperature to room temperature and subsequently, for a number of thermal cycles. The temperature values used during the cycles are typical of those actually used in thermal cycling at The University of Tennessee Space Institute. From the calculated matrix stress, the fiber stress and strain and the matrix strain components were also obtained by the use of Eqs. (2), (8), (10), and (13).

The equation solved by the program, Eq. (14), to obtain the matrix stress is restated here:

$$\int_{T_1}^{T_2} (\alpha_m - \alpha_f)\,dT = \frac{\sigma_a - \sigma_m}{V_f E_f} - \left\{ \frac{\sigma_m}{E_m} \pm \left[\frac{\sigma_m - \sigma_o}{K_*} \right]^{\frac{1}{n}} \right.$$

$$\left. \pm \int_{T_1}^{T_2} A\left(\frac{|\sigma_m|}{G} \right)^S \frac{Gb}{kT} D_o e^{-Q/RT} \left(\frac{dt}{dT}\right) dT \right\} . \qquad (14)$$

Values for the temperature dependent properties, α_m , E_m , σ_o , G, and Q, were obtained by linearly interpolating between tabulated values. The fiber properties, α_f and E_f , were assumed to be temperature independent. Values for the constants, K_* , n, A, S, and D_o , as taken from Garmong, are:

$$K_* = 1.0 \times 10^5 \text{ psi} ,$$

$$n = 0.5 ,$$

$$S = 4.4 ,$$

$$A \cdot D_o = 8.837 \times 10^5 \ \frac{\text{in.}^2}{\text{sec}^\circ\text{K}} .$$

The matrix stress was assumed to be zero at 500°C and was calculated for successive small temperature changes by use of the bisection method [31]. The integrals were evaluated by use of the trapezoidal rule [31]. A flow-chart of the computer program is given in Figure 19.

A number of assumptions are made in these calculations. The major ones are that:

1. The composite is essentially one-dimensional.
2. Stresses and strains are uniform within each phase.
3. No interphase sliding occurs.
4. The composite is metallurgically and thermodynamically stable.
5. Plastic stress-strain and creep relations and yield stress are the same for both tension and compression.

6. Strain hardening is annealed out between successive thermal cycles.

7. The effect of long hold times at room temperature is not taken into account.

The 2024 alloy was used for the matrix in these calculations because of the availability of property data. Two cycle rates, 6 and 12 minutes/cycle, were evaluated in order to determine the effect of frequency. The constant cooling rate from fabrication temperature was somewhat arbitrarily chosen to be 1°C per second.

The calculated matrix stress versus temperature for 12 minutes/cycle is shown in Figure 20. It may be seen that only two cycles are required to produce a steady hysteresis loop. As the temperature decreases from 500°C at fabrication, the matrix tends to contract but is constrained by the fibers, producing a tensile stress. The matrix stress increases slowly at first because of stress relief by creep. But by about 100°C the ability to creep is greatly reduced and the stress rises sharply, exceeding the yield point. As the temperature rises again during the subsequent thermal cycles, the tensile stress falls off rapidly as the matrix expands. But now it is compressed by the fiber restraint, reaching a peak compressive stress at 150°C. At this point creep becomes sufficient to provide stress relief so that the matrix stress decreases toward zero as the temperature continues to increase. The cooling rate from a maximum cyclic temperature of 425°C is slow enough that creep

prevents the matrix stress from again exceeding the yield point. The cyclic stress limits are shown to be 11 ksi tensile and 5 ksi compressive, a stress range of 16 ksi.

The stress versus strain curve is indicated in Figure 21. Upon heating from the lower cyclic temperature limit, the curve initially decreases linearly, indicating elastic strain. At the compressive peak creep begins to return the matrix back to equilibrium with the fibers. The strain rate is initially rapid on cooling due to creep. But at about 100°C, it decreases with decreased creep until the low temperature limit is again reached.

Figure 22 shows the creep strain as a function of temperature. As the temperature increases from near room temperature, the tensile creep strain in the matrix is unchanged until 150°C is reached; that is, negligible creep occurs. After 150°C the creep strain decreases at a constant rate of 24 μ inch/inch per °C to a minimum at the upper temperature.

The fiber stresses as a function of temperature are shown in Figure 23. They are slightly higher than the matrix stresses because a 45% of fibers was used.

The curves for the 6 minutes/cycle stresses and strains, Figures 24 and 25, are seen to be almost identical to those of 12 minutes/cycle, except that the maximum tensile stress and strain are less because of a higher

minimum temperature. The reason for this would seem to be that the calculated creep strain is dominated by temperature rather than time.

Composite Degradation

Boron-aluminum composites have very high tensile strength to density ratios in their undegraded condition. Typical as-received values of strength (Tables 1, 2, and 3) and specific gravity (Table 5) are 210 ksi and 2.62, giving a specific strength of about 80 ksi. In comparison, the value for 2024-T4 aluminum would be 24 ksi, 12 ksi for cold drawn 1045 steel, and about 19 ksi for Inconel. Even for a titanium alloy such as Ti-6Al-4V, the value would be only about 37 ksi [32]. At short time elevated temperatures the strength to weight superiority of B-Al is even greater since its strength falls off with increasing temperature less rapidly than that of most metals [33, 34].

The high strength of a metal matrix composite such as B-Al is dependent upon maintaining the integrity of the fibers, the interface, and the matrix [35, 28]. If the matrix delaminates, becomes broken up or reacted, its ability to transfer loads to the fibers is diminished. The interface serves as the bond between fibers and matrix, the zone of stress transfer, and as a protective barrier against reaction. A thick reaction layer at the interface will decrease its load transfer capability and the bond strength. Cracks in the interfacial layer reduce its efficiency, act

as crack starters for the fibers, and interrupt the barrier against interdiffusion and access of reactive species to the fibers.

Boron-aluminum held at elevated temperatures for various lengths of time have been shown to be degraded. In work by Wright and Intwala [1], 50% fiber specimens held at 600°C for one hour showed an approximately 50% tensile strength loss. Holding for subsequent lengths of time resulted in a slower rate of strength reduction. The strength loss was attributed to fiber and interface degradation.

Coating of boron fibers with silicon carbide has been used extensively to provide a barrier against reaction at high temperature. Dardi and Krieder [2] report that while a B-Al composite containing uncoated fibers exhibited a 12% longitudinal strength decrease after 1,000 hours at 370°C, a Borsic-Al composite showed no strength decrease. Other means of protecting boron fibers are by deposited coatings of B_4C, BN, or TiB_2 [36].

Several researchers have reported the detrimental influence of thermal cycling in air on B-Al composites. Shananian [3] cycled 2024 and 6061 Al-B between near room temperature and 300 or 500°C. Surface roughening was reported which was more extensive in the 2024 aluminum matrix. Both matrices developed surface cracks that exposed the fibers. Specimens cycled to 500°C for 2,000 cycles showed more strength reduction than did those cycled to

300°C. Increasing the cyclic frequency from three to one minute per cycle was reported to result in 10% less strength loss.

That thermal cycling damage is dependent upon high temperatures was also demonstrated by Shahanian. Experiments in which B-Al was cycled between 10 and -186°C resulted in no cracking or strength loss despite the presence of higher thermal stresses and strains.

The thermal cycling observations of Shahanian with regard to the effects of temperature, matrix alloy type, and cyclic frequency have been supported by the work of Wright [4, 12]. He also studied the effects of various ply orientations, fiber volume fractions, applied loads, and pre-machined notches. Somewhat more severe surface roughening was reported for cross-plied specimens, due presumably to the complex stress state. The effect of volume fraction was found to be small. Fracture studies indicated a reduction in fracture toughness and a change of failure mode from crack propagation to bundle failure.

Damage Mechanisms

Matrix. In the past most investigations of both mechanical fatigue and thermal cycling have been conducted in air and the effect of the environment has been generally ignored.

The fact that significantly less matrix degradation was apparent in this investigation when boron-aluminum was thermally cycled in argon rather than in air indicates an environmentally controlled phenomena such as corrosion fatigue. As pointed out in Chapter II, corrosion fatigue is a general term for environmentally enhanced fatigue damage. The processes being enhanced and the processes by which enhancement occurs may vary greatly depending upon the situation.

As seen in Figures 20 and 24 of the appendix, the calculated steady-state matrix stress does not reach the yield stress for the cyclic conditions considered. Therefore, there is no gross time independent plastic flow. Fatigue can, however, occur at gross stresses well below the yield stresses due to localized plastic flow at microstructural stress concentrations and at soft spots in the grains. The extent of this deformation is insufficient to cause fatigue failure of the matrix within a few thousand cycles.

The cyclic strain amplitude in the matrix, on the other hand, is quite large, as seen in Figure 22. For the case shown it is 6,900 μ inch/inch or about 0.7%. Therefore, due to its large magnitude the cyclic creep strain would be expected to be the basic source of matrix damage, rather than the stress or the time independent plastic strain. Reversed creep could account for the surface cracking, roughening, and ratcheting that is observed. In

the cycled composites the matrix surface cracks appear to be intergranular. This is in agreement with the fact that creep cracking is almost always intergranular.

The Manson-Coffin relation, Eq. (15), is useful for estimation of low-cycle fatigue life based on the time independent plastic strain per cycle. However, it is not expected to be applicable to cyclic creep fatigue, which does not have the same dependence on the metal ductility.

It is proposed that one or more of the corrosion fatigue mechanisms outlined in Chapter II account for the increased amounts of surface roughening and cracking and the formation of internal cracks and voids when B-Al is thermally cycled in air. Either adsorbed gas, oxide films, or hydrogen embrittlement would decrease the capability of the surface layer to accommodate plastic strains and aid in the initiation and subsequent propagation of cracks into the surface. Once the surface becomes discontinuous, its surface tension may cause it to ball up or form nodules.

Once cracks initiate in the surface layer, the remainder of the matrix effective life is spent in propagating these cracks into the interior. The relative importance of the environment during the initiation and propagation phases could only be determined by experiment. However, it is expected to play an important role in both. The fact that very few fibers extracted from air cycled specimens show strengths as high as the average as-received

strength indicate that almost all have been exposed to the air by extensive crack propagation into the composite.

The observed effects of temperature, cyclic frequency, and alloy type correlate well with the corrosion fatigue model. Since corrosion fatigue is dependent upon both temperature and time, the greatest damage would be expected at high temperature and low cyclic frequency, as is observed. Alloying is believed to increase the extent of corrosion fatigue by such mechanisms as galvanic effects, increased internal energy, and creep interference leading to higher stresses.

Water vapor in the air is most likely the principal environmental agent in thermal corrosion fatigue of the matrix, as it has been shown to be in mechanical corrosion fatigue of aluminum. It is presumed that the water vapor partial pressure in the argon atmosphere was below the transition pressure for the existing stress level.

Fibers and interface. The observation that fibers extracted from air cycled specimens are weaker than those from argon cycled specimens may be explained in two ways: (1) The more extensive matrix damage during air cycling causes more cracks to be formed in the aluminum diboride layer on the fibers. These cracks serve as stress concentrators and weaken the fibers. (2) Exposure to the air of fibers with aluminum diboride layers already disrupted by matrix cracking results in localized severe oxidation at

high temperature. These reaction sites act as crack starters and lower the fiber strength.

Either oxygen or water vapor in the environment could result in fiber oxidation. Since they are both present in the air, fiber oxidation is attributed to their combined action.

CHAPTER VI

CONCLUSIONS

1. Boron-aluminum composites thermally cycled to a maximum temperature of 425°C for 6,000 cycles exhibited large longitudinal and transverse strength degradations in air but not in argon.

2. Fibers extracted from specimens thermally cycled in argon showed little or no strength decrease while those from air cycled specimens showed decreases as high as almost 50%.

3. Cycling in air produced a greater amount of surface roughening and cracking than did cycling in argon.

4. The greatest amount of matrix damage was indicated by the 2024 material and the least by the 1100 material.

5. The greatest strength degradation of composite and fibers was for the 6061 material, presumably because of its originally inferior fibers. The 1100 material showed the least strength degradations.

6. Density measurements indicated more void formation on specimens thermally cycled in air than in argon.

7. Increased matrix degradation in air was attributed to corrosion fatigue due to the presence of water vapor.

8. Lower fiber strengths and consequent composite strengths were believed to result from either fiber oxidation or more extensive interfacial layer breakup.

CHAPTER VII

RECOMMENDATIONS

1. Experiments are needed to further substantiate the corrosion fatigue hypothesis and to positively identify the active atmosphere agent. Such experiments might be to provide corrosion protection to air cycled specimens, thermal cycling in argon containing different amounts of moisture, and thermal cycling in dry air.

2. Microscopic study should be made of the early stages of matrix degradation to determine the crack path and the effect of precipitate particles.

3. More computer calculations are needed of the effect of different cyclic conditions and different composite properties on the stresses and strains generated.

4. All age hardenable matrix composites should be pre-annealed before cycling or testing.

BIBLIOGRAPHY

BIBLIOGRAPHY

1. Wright, M. A., and B. Intwala. "The Effect of Elevated Temperatures on the Mechanical Properties of B-Al Composites," Journal of Material Science, Part VIII, 7:957-963, July, 1973.

2. Dardi, L. E., and K. G. Kreider. "Effect of Salt Water and High Temperature Exposure on Boron-Aluminum Composites," Composite Materials: Testing and Design (Third Conference). ASTM Special Technical Publication No. 546. Philadelphia: American Society for Testing and Materials, 1974. Pp. 269-283.

3. Shahanian, P. "Thermal Fatigue of Boron-Aluminum Composites," SAMPE Quarterly, 2:28-35, June, 1970.

4. Wright, M. A. "The Effects of Elevated Temperatures on the Structural Properties of Fiber Composite Materials Suitable for Use in Space Shuttle and Other Space Vehicles." Final report prepared under NASA Contract No. UT 844001-6463R-95 by The University of Tennessee Space Institute, Tullahoma, Tennessee, October, 1972.

5. Ebert, L. J., and P. K. Wright. "Mechanical Aspects of the Interface," Composite Materials - Volume 1, Interfaces in Metal Matrix Composites. A. G. Metcalfe, editor. New York: Academic Press, Inc., 1974. Pp. 31-64.

6. Wills, J. L. "The Effects of Thermal Cycling on Boron-Aluminum Composites." Unpublished Master's thesis, The University of Tennessee, Knoxville, 1972.

7. Garmong, G. "Elastic-Plastic Analysis of Deformation Induced by Thermal Stress in Eutectic Composites," Metallurgical Transactions, 5:2183-2205, October, 1974.

8. DeSilva, A. R. T., and G. A. Chadwick. "Thermal Stresses in Fibre Reinforced Composites," Journal of Mechanics and Physics of Solids, 17:387-403, 1969.

9. Kreider, K. G., L. Dardi, and K. Prewo. "Metal Matrix Composite Technology," Air Force Materials Laboratory TR-71-204, Wright-Patterson Air Force Base, Ohio, December, 1971.

10. Taira, S. "Thermal Fatigue and Its Relation to Creep Rupture and Mechanical Fatigue," High Temperature Structures and Materials--Proceedings of the Third Symposium on Naval Structural Mechanics. A. M. Freudenthal, B. A. Boley, and H. Liebowitz, editors. New York: Pergamon Press, 1964. Pp. 187-213.

11. Dieter, G. E. Mechanical Metallurgy. Metallurgy and Metallurgical Engineering Series, R. F. Mehl and M. B. Bever, editors. New York: McGraw-Hill Book Company, Inc., 1961.

12. Wright, M. A. "The Mechanical Properties of Metal Matrix Composites Subjected to Cyclic Temperature Changes." Technical Report prepared under Navy Contract No. N0014-71-A-0121-0003 NR 031-760 by The University of Tennessee Space Institute, Tullahoma, Tennessee, October, 1974.

13. Dorn, J. E. "Basic Aspects and Physical Theories of Creep of Metals," Materials Engineering Design for High Temperatures. J. Marin, editor. Proceedings of a short course conducted at The Pennsylvania State University, June, 1958.

14. Fontana, F. G., and N. D. Greene. Corrosion Engineering. New York: McGraw-Hill Book Company, Inc., 1967.

15. Duquette, D. J. "A Review of Aqueus Corrosion Fatigue," Corrosion Fatigue: Chemistry, Mechanics and Microstructure. Houston, Texas: National Association of Corrosion Engineers, 1972. Pp. 12-24.

16. Wei, R. P. "Some Aspects of Environmental-Enhanced Fatigue-Crack Growth," Journal of Engineering Fracture Mechanics, 1:633-651, 1970.

17. Hockenhull, B. S., H. A. Monks, and H. Sala. "Frequency and Environmental Interactions in the Fatigue of Aluminum Alloys," Corrosion Fatigue: Chemistry, Mechanics and Microstructure. Houston, Texas: National Association of Corrosion Engineers, 1972. Pp. 453-458.

18. Krupp, W. E., D. W. Hoeppner, and E. K. Walker. "Crack Propagation of Aluminum Alloys in Corrosive Environments," Corrosion Fatigue: Chemistry, Mechanics and Microstructure. Houston, Texas: National Association of Corrosion Engineers, 1972. Pp. 468-483.

19. Feeney, J. A., J. C. McMillan, and R. P. Wei. "Environmental Fatigue Crack Propagation of Aluminum Alloys at Low Stress Intensity Levels," Metallurgical Transactions, 1:1741-1757, June, 1970.

20. Broom, T., and A. Nicholson. "Atmospheric Corrosion-Fatigue of Age-Hardened Aluminum Alloys," Journal of the Institute of Metals, 89:183-190, 1961.

21. Grosskrentz, J. C. "Corrosion Fatigue of Aluminum Alloys--Critical Introduction," Corrosion Fatigue: Chemistry, Mechanics and Microstructure. Houston, Texas: National Association of Corrosion Engineers, 1972. Pp. 451-452.

22. Wadsworth, N. J., and J. Hutchings. "The Effect of Atmospheric Corrosion Metal Fatigue," Philosophical Magazine, 3:1154-1166, 1958.

23. Enochs, J. S., and O. F. Devereaux. "Fatigue Crack Growth in 5052-H34 Aluminum in Vacuum and Active Gas Environments," Metallurgical Transactions, 6A:391-397, February, 1975.

24. Grosskrentz, J. C. "The Effect of Surface Films on Fatigue Crack Initiation," Corrosion Fatigue: Chemistry, Mechanics and Microstructure. Houston, Texas: National Association of Corrosion Engineers, 1972. Pp. 201-210.

25. Smith, H. H., and P. Shahanian. "Effect of Water Vapor on Fatigue Behavior of an Aluminum-Boron Composite," Corrosion Fatigue: Chemistry, Mechanics and Microstructure. Houston, Texas: National Association of Corrosion Engineers, 1972. Pp. 499-505.

26. Klein, M. J., and A. G. Metcalfe. "Effect of the Interfaces in Metal Matrix Composites on Mechanical Properties," Air Force Materials Laboratory TR-71-189, Wright-Patterson Air Force Base, Ohio, October, 1971.

27. Louthan, M. R., and A. H. Dexter. "Hydrogen Embrittlement of 1100 Aluminum," Metallurgical Transactions, 6A:1655-1657, August, 1975.

28. Metcalfe, A. G. "Physical Chemical Aspects of the Interface," Composite Materials - Volume 1, Interfaces in Metal Matrix Composites. A. G. Metcalfe, editor. New York: Academic Press, Inc., 1974. Pp. 31-64.

29. Galasso, F. S. High Modulus Fibers and Composites. New York: Gordon and Breach, Science Publishers, Inc., 1969.

30. Welch, D. Private communication. The University of Tennessee Space Institute, Tullahoma, Tennessee, 1976.

31. Hamming, R. W. Introduction to Applied Numerical Analysis. New York: McGraw-Hill Book Company, Inc., 1971.

32. Bolz, R. E., and G. L. Tuve (editors). Handbook of Tables for Applied Engineering Science. Cleveland, Ohio: The Chemical Rubber Company, 1970.

33. Meyn, D. A. "Effect of Temperature and Strain Rate on the Tensile Properties of Boron-Aluminum and Boron-Epoxy Composites," Composite Materials: Testing and Design (Third Conference). ASTM Special Technical Publication No. 546. Philadelphia: American Society for Testing and Materials, 1974. Pp. 225-236.

34. Sessler, J. G., and V. Weiss (editors). Aerospace Structural Metals Handbook - Volume 2, Nonferrous Alloys. Air Force Materials Laboratory TR-68-115. Wright-Patterson Air Force Base, Ohio: Air Force Materials Laboratory, 1968.

35. Cooper, G. A., and A. Kelly. "Role of the Interface in the Fracture of Fiber-Composite Materials," Interfaces in Composites. ASTM Special Technical Publication No. 452. Philadelphia: American Society for Testing and Materials, 1969. Pp. 90-106.

36. Naslain, R., J. Thebault, and R. Pailler. "Chemical Compatibility in Metal-Boron Composites," Proceeding of the 1975 International Conference on Composite Materials - Volume 1. New York: The American Institute of Mining, Metallurgical, and Petroleum Engineers, Inc., 1976. Pp. 116-136.

APPENDIX

Table 1

Measured Mechanical Properties of 6061 Matrix B-Al Composite

Matrix	Orientation	Cycle Period (min.)	Atm.	UTS[a] (ksi)	ΔUTS (%)	$E_{11}x10^{-6}$ (psi)	$E_{22}x10^{-6}$ (psi)	ν_{21}	ν_{12}
6061	Long.	AR	-	171.0	-	40.3	-	0.242	-
		6	Inert	175.6	+2.7	33.3	-	0.230	-
		12	Inert	184.4	+7.8	34.3	-	0.250	-
		12	Air	59.9	-65.0	32.7[a]	-	0.221	-
6061	Trans.	AR	-	16.4	-	-	17.9	-	0.100
		6	Inert	15.0	-8.5	-	17.9	-	0.118
		12	Inert	12.6	-23.2	-	15.0	-	0.106
		12	Air	11.3[b]	-31.1	-	15.2	-	0.154

[a] Average of two specimens.

[b] [30].

Table 2

Measured Mechanical Properties of 2024 Matrix B-Al Composite

Matrix	Orientation	Cycle Period (min.)	Atm.	UTS (ksi)	ΔUTS (%)	$E_{11} \times 10^{-6}$ (psi)	$E_{22} \times 10^{-6}$ (psi)	ν_{21}	ν_{12}
2024	Long.	AR	-	206.0[a]	-	36.4	-	0.250	-
	Long.	6	Inert	209.9[a]	+1.9	32.1	-	0.237	-
	Long.	12	Inert	210.0[a]	+1.9	31.6	-	0.250	-
	Long.	12	Air	80.3[a]	-61.0	38.8[a]	-	0.243	-
2024	Trans.	AR	-	38.0[a]	-	-	19.6	-	0.099
	Trans.	6	Inert	14.4[a]	-62.1	-	21.0	-	0.129
	Trans.	12	Inert	10.7[a]	-71.8	-	9.4[a]	-	0.105
	Trans.	12	Air	8.6	-77.4	-	16.5	-	0.104

[a]Average of two specimens.

Table 3

Measured Mechanical Properties of 1100 Matrix B-Al Composite

Matrix	Orientation	Cycle Period (min.)	Atm.	UTS (ksi)	ΔUTS (%)	$E_{11} \times 10^{-6}$ (psi)	$E_{22} \times 10^{-6}$ (psi)	ν_{21}	ν_{12}
1100	Long.	AR	-	192.1[a]	-	33.8	-	0.247	-
	Long.	6	Inert	186.5[a]	-2.9	30.9	-	0.236	-
	Long.	12	Inert	196.1[a]	+2.1	30.5	-	0.238	-
	Long.	12	Air	108.4[a]	-43.6	30.5[a]	-	0.233	-
1100	Trans.	AR	-	8.1[a]	-	-	17.5	-	0.147
	Trans.	6	Inert	6.1[a]	-24.7	-	12.9	-	0.103
	Trans.	12	Inert	6.0[a]	-25.9	-	12.7[a]	-	0.057
	Trans.	12	Air	4.3	-46.9	-	11.1	-	

[a]Average of two specimens.

Table 4

Experimental Data for Extracted 2 Inch Long Boron Fibers

Matrix	Period (min.)	Atm.	$\bar{\sigma}_A$(ksi)	$\bar{\sigma}_G$(ksi)	$\bar{\sigma}_W$(ksi)	ω	σ_o(ksi)	Coeff. of Variation	$(\Delta\bar{\sigma}_W)$ %
6061[a]	AR[b]	-	432.8	412.4	424.4	9.943	832	0.121	-
	6	Argon	434.4	424.5	427.4	11.292	773	0.107	+0.7
	12	Argon	421.6	371.4	413.9	7.573	992	0.156	-2.5
	12	Air	231.3	213.4	222.8	6.254	640	0.187	-47.5
2024[c]	AR	-	514.0	490.8	505.9	13.231	818	0.092	-
	6	Argon	503.8	491.5	495.1	14.846	760	0.083	-2.2
	12	Argon	471.6	436.6	459.8	11.509	799	0.105	-9.1
	12	Air	363.8	345.4	388.9	2.763	361	0.391	-23.1
1100[c]	AR	-	436.0	372.8	428.0	6.219	1,180	0.188	-
	6	Argon	436.7	424.6	426.7	8.587	891	0.139	-0.3
	12	Argon	438.2	427.8	426.8	7.743	964	0.153	-0.3
	12	Air	361.7	344.0	352.2	8.748	725	0.137	-17.7

[a] 4.0 mil diameter fibers.

[b] AR = As received.

[c] 5.8 mil diameter fibers.

Table 5

Density Measurements of As-Received and Thermally Cycled B-Al

Matrix	Orien-tation	Cycle Period (min.)	Atmosphere	Density (gm/cm^3)	Δ Density (%)
6061	Long.	AR	-	2.6411	-
6061	Long.	6	Inert	2.6333	-0.30
6061	Long.	12	Inert	2.6540	+0.49
6061	Long.	12	Air	2.5627	-2.97
6061	Trans.	AR	-	2.6198	-
6061	Trans.	6	Inert	2.6376	+0.68
6061	Trans.	12	Inert	2.6272	+0.28
2024	Long.	AR	-	2.6380	-
2024	Long.	6	Inert	2.6266	-0.43
2024	Long.	12	Inert	2.6304	-0.29
2024	Long.	12	Air	2.5974	-1.54
2024	Trans.	AR	-	2.6253	-
2024	Trans.	6	Inert	2.6075	-0.68
2024	Trans.	12	Inert	2.6168	-0.32
2024	Trans.	12	Air	2.5808	-1.72
1100	Long.	AR	-	2.5944	-
1100	Long.	6	Inert	2.5367	-2.22
1100	Long.	12	Inert	2.5830	-0.44
1100	Long.	12	Air	2.4463	-5.71
1100	Trans.	AR	-	2.6039	-
1100	Trans.	6	Inert	2.5970	-0.46
1100	Trans.	12	Inert	2.5538	-1.96
1100	Trans.	12	Air	2.4600	-5.53



Figure 1. The sub-surface of a boron-aluminum specimen after 6,000 cycles in air.

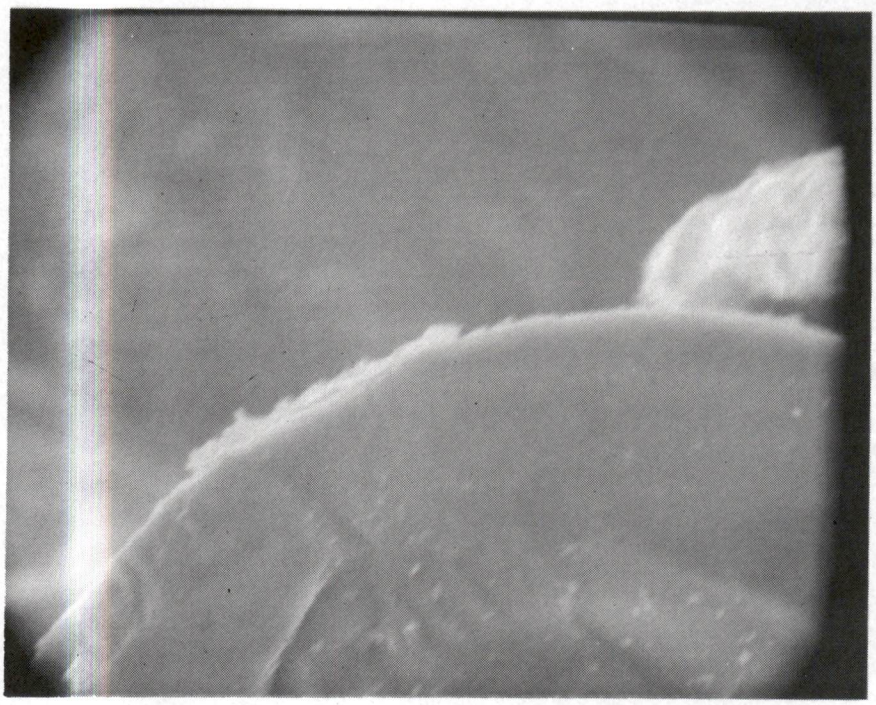

Figure 2. An apparent oxide film at the interface of as-received boron-aluminum.

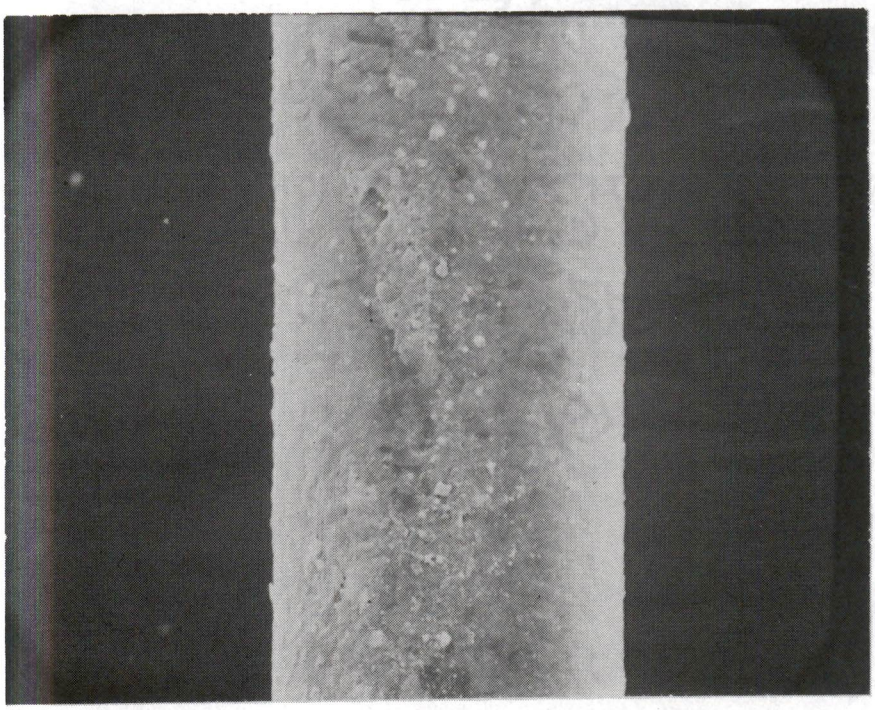

Figure 3. A boron fiber covered with reaction products.

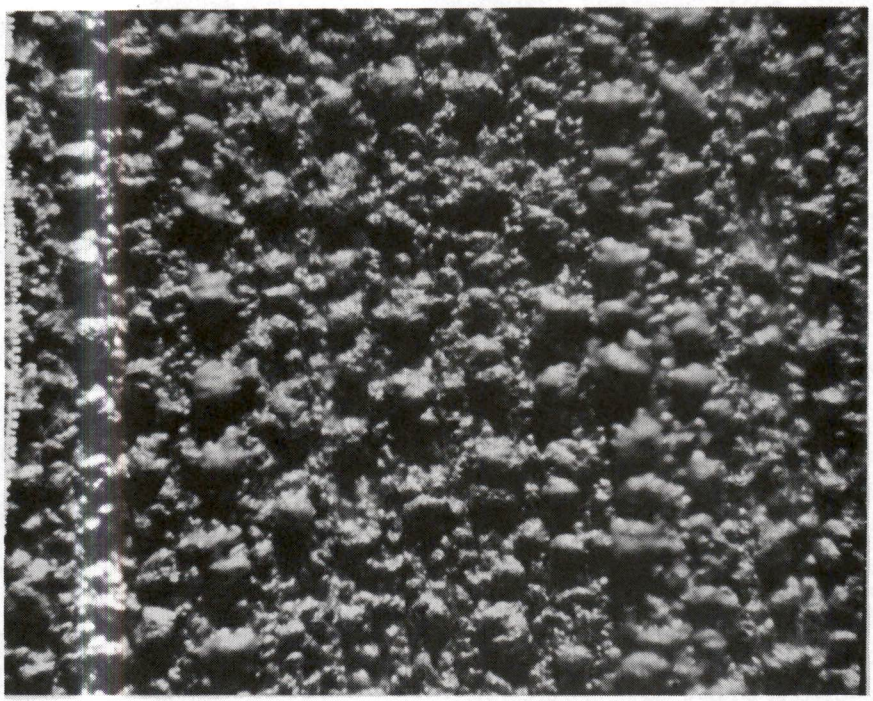

Figure 4. The spheroidazation of a thermally cycled boron-aluminum surface.

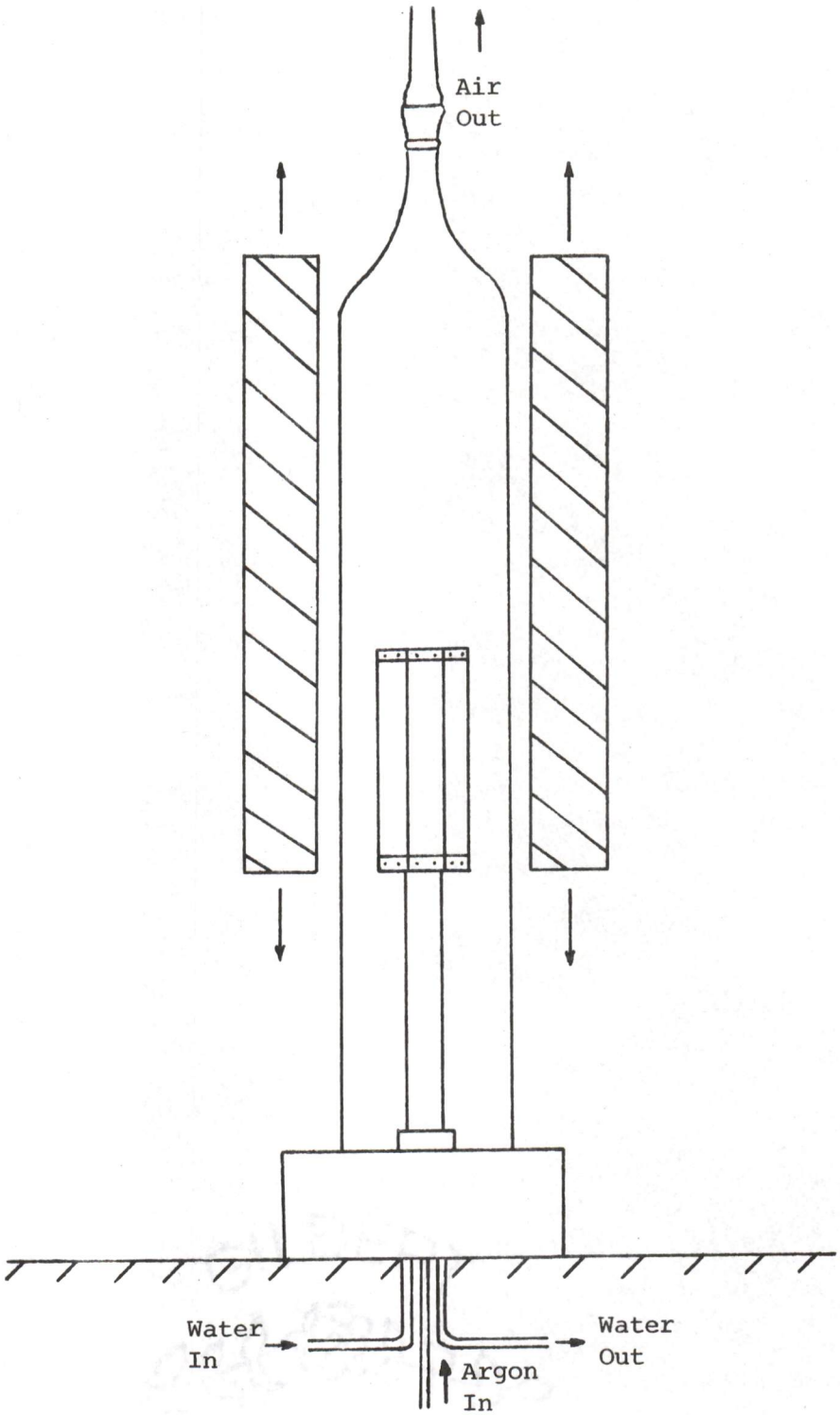

Figure 5. A diagram of the controlled atmosphere thermal cycling furnace.

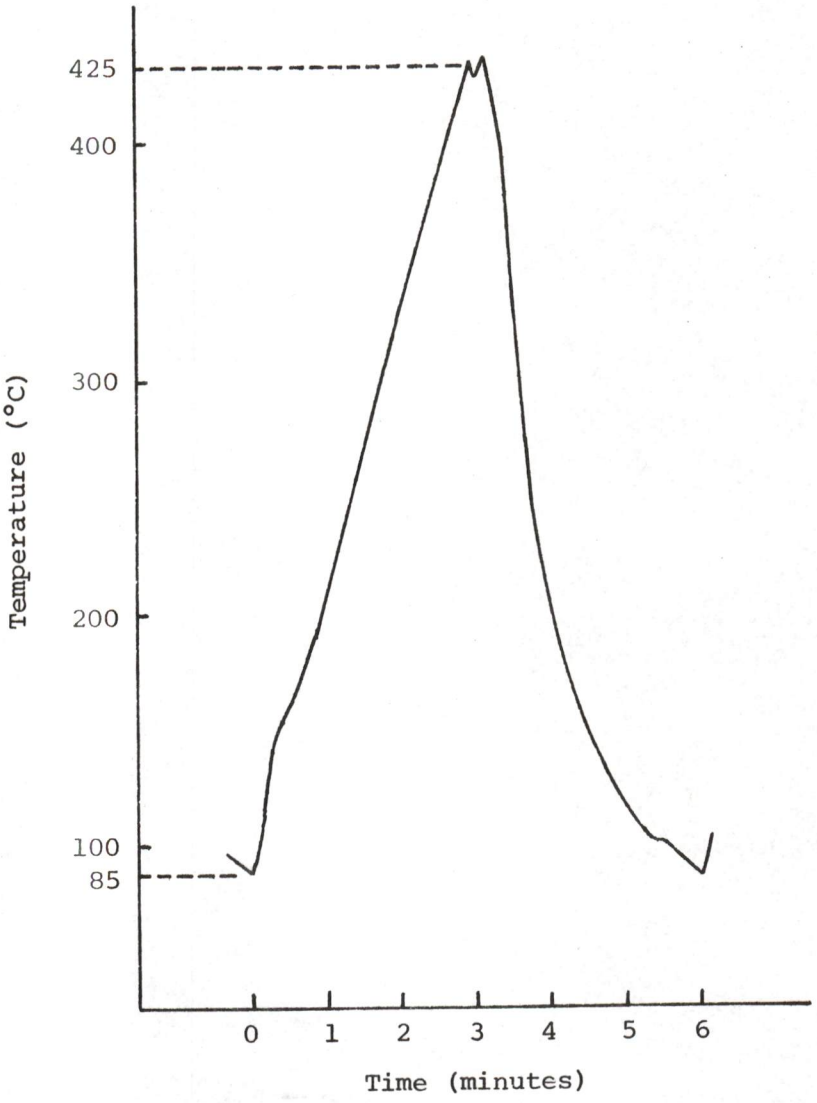

Figure 6. The specimen temperature during thermal cycling, 6 minutes/cycle.

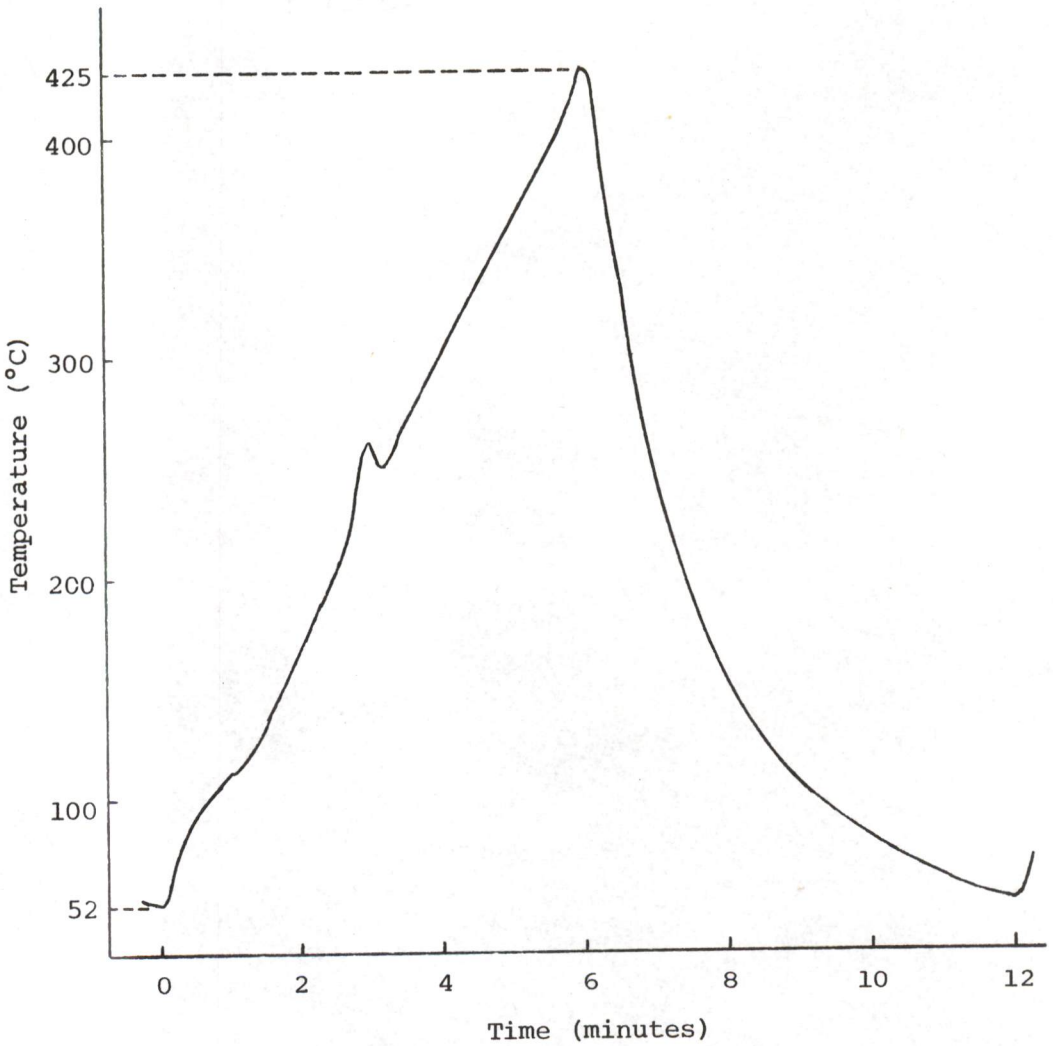

Figure 7. The specimen temperature during thermal cycling, 12 minutes/cycle.

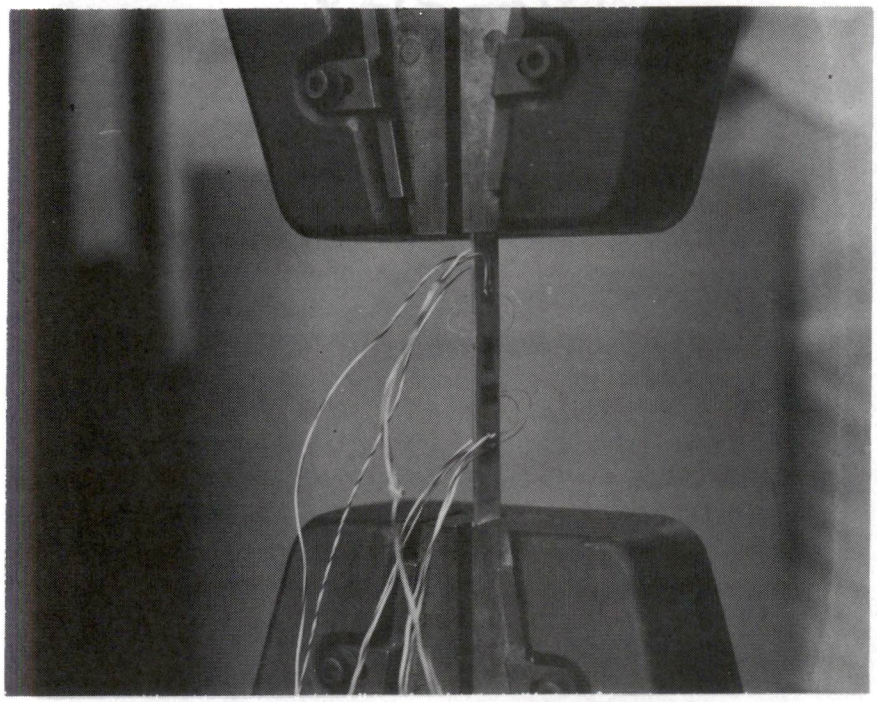

Figure 8. An instrumented composite specimen gripped in the tensile machine.



Figure 9. A typical fracture surface of 6061 aluminum-boron.

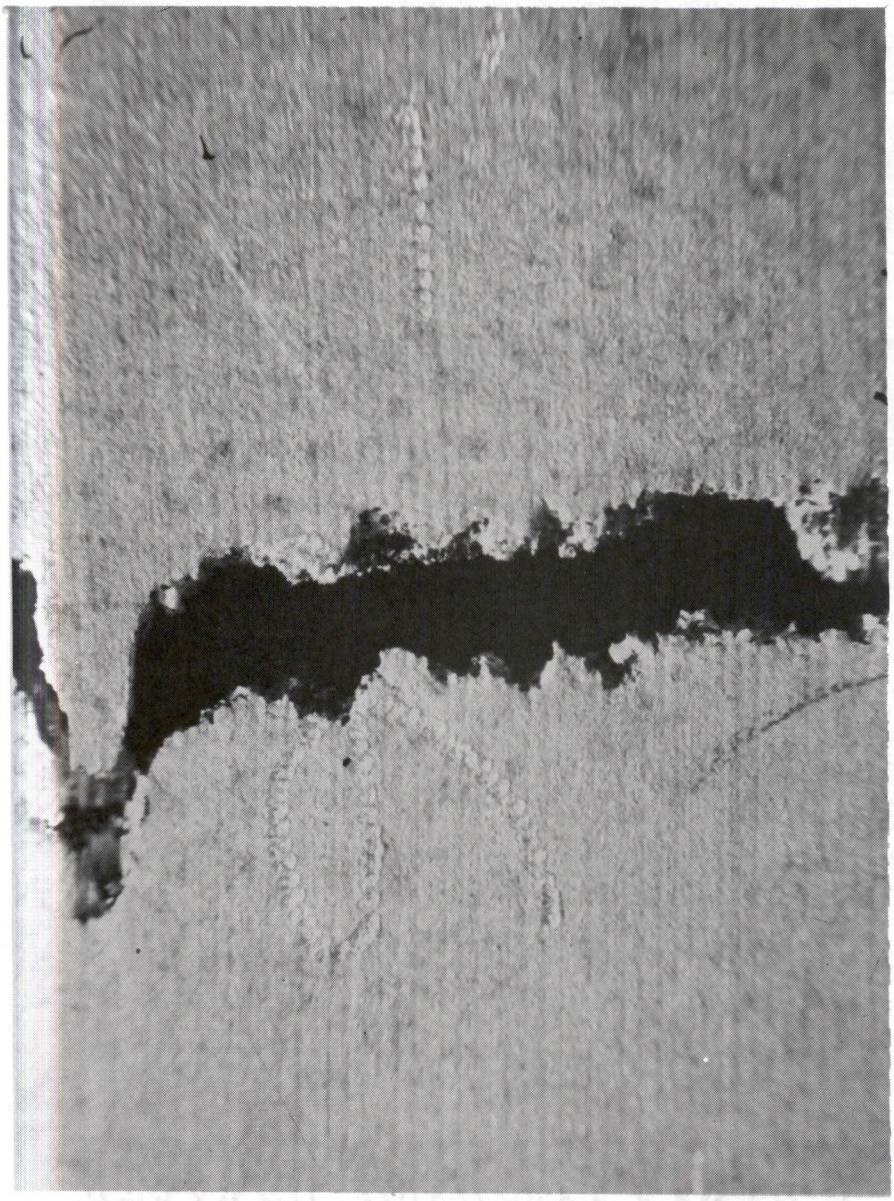

Figure 10. A typical fracture surface of 2024 aluminum-boron.

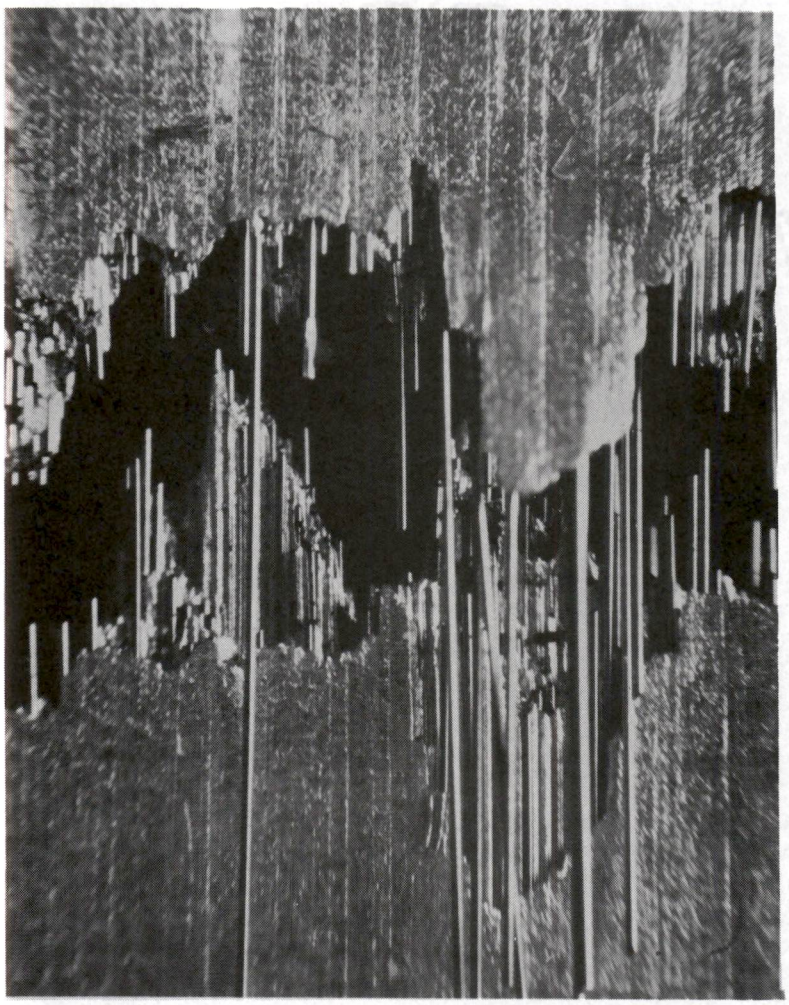

Figure 11. A typical fracture surface of 1100 aluminum-boron.

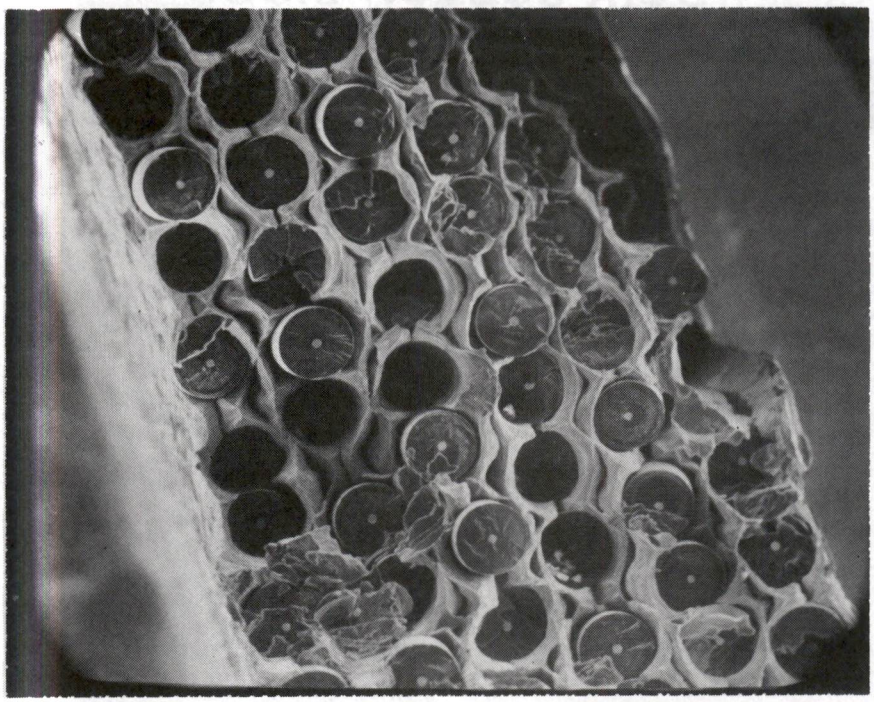

Figure 12. A micrograph showing the poor consolidation of the 1100 aluminum-boron.

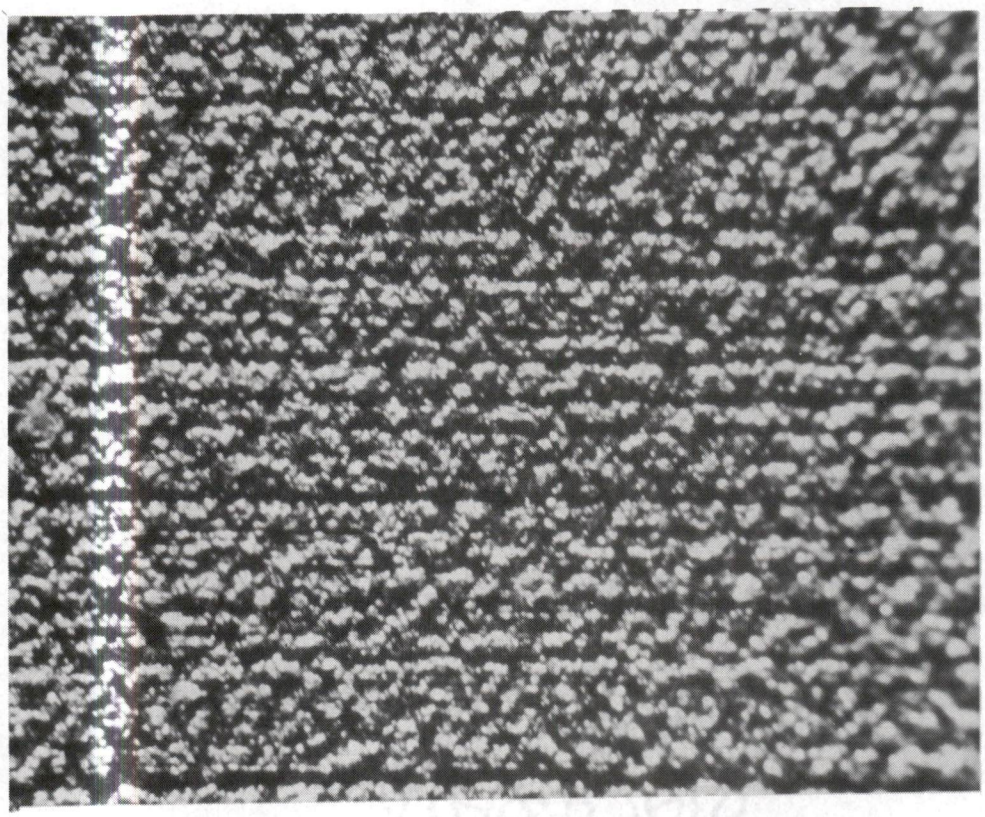

Figure 13. The surface of 6061 aluminum-boron thermally cycled in argon, 12 minutes/cycle.

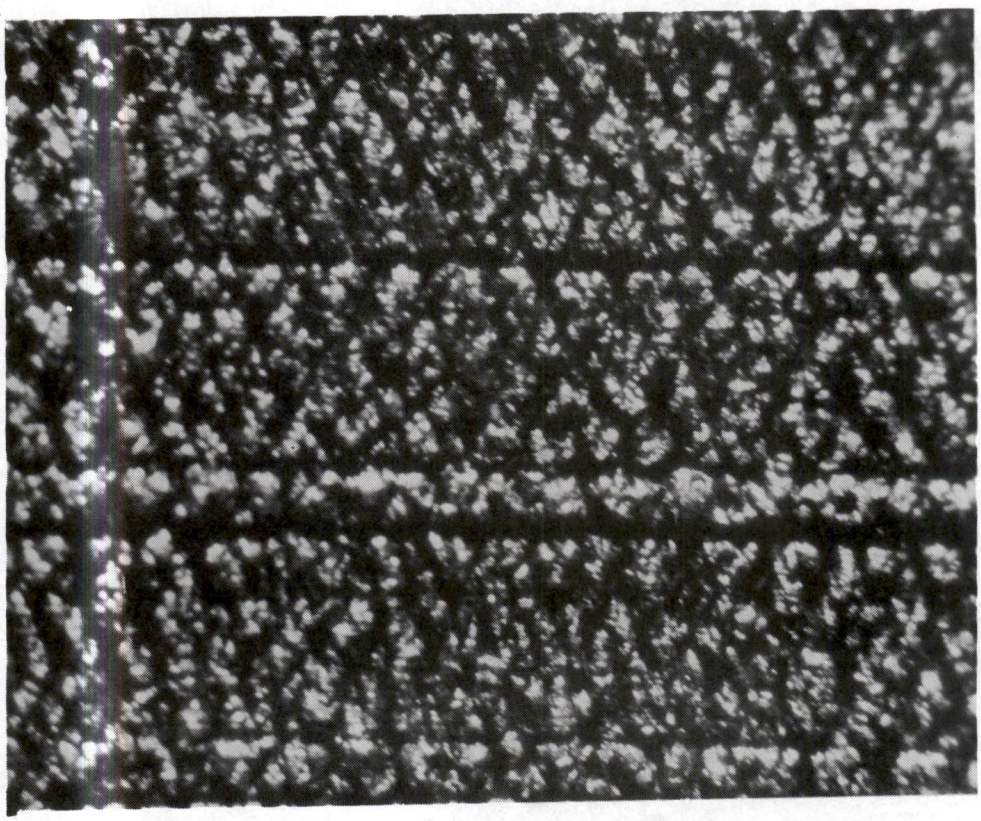

Figure 14. The surface of 6061 aluminum-boron thermally cycled in air, 12 minutes/cycle.

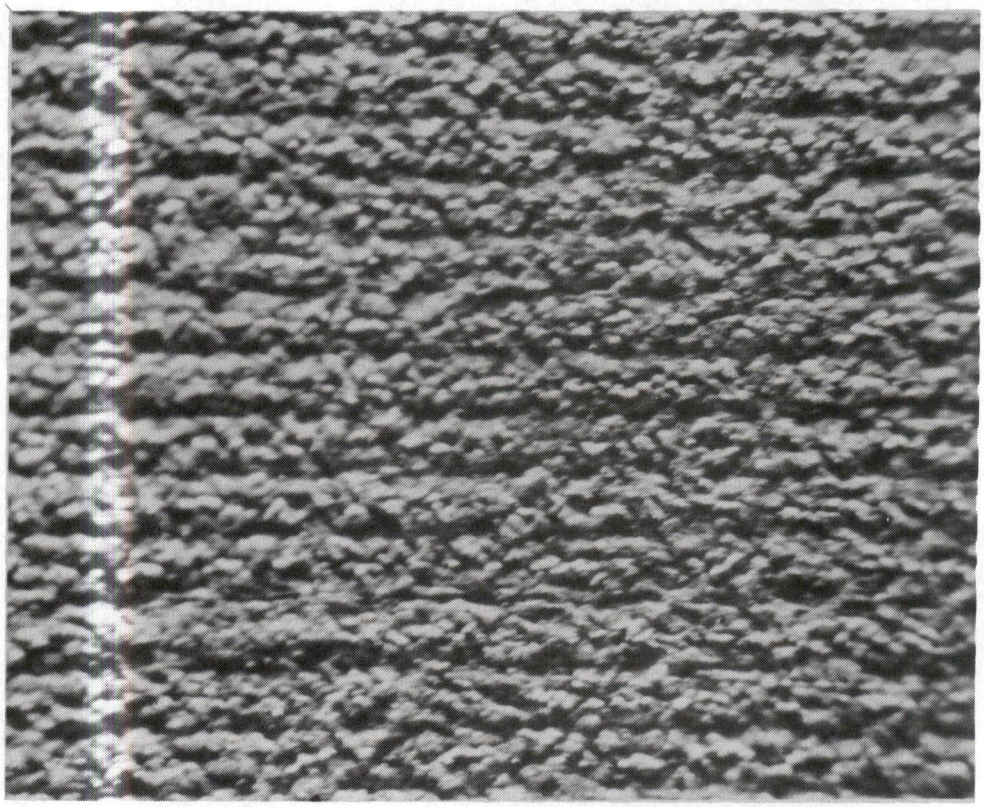

Figure 15. The surface of 2024 aluminum-boron thermally cycled in argon, 12 minutes/cycle.

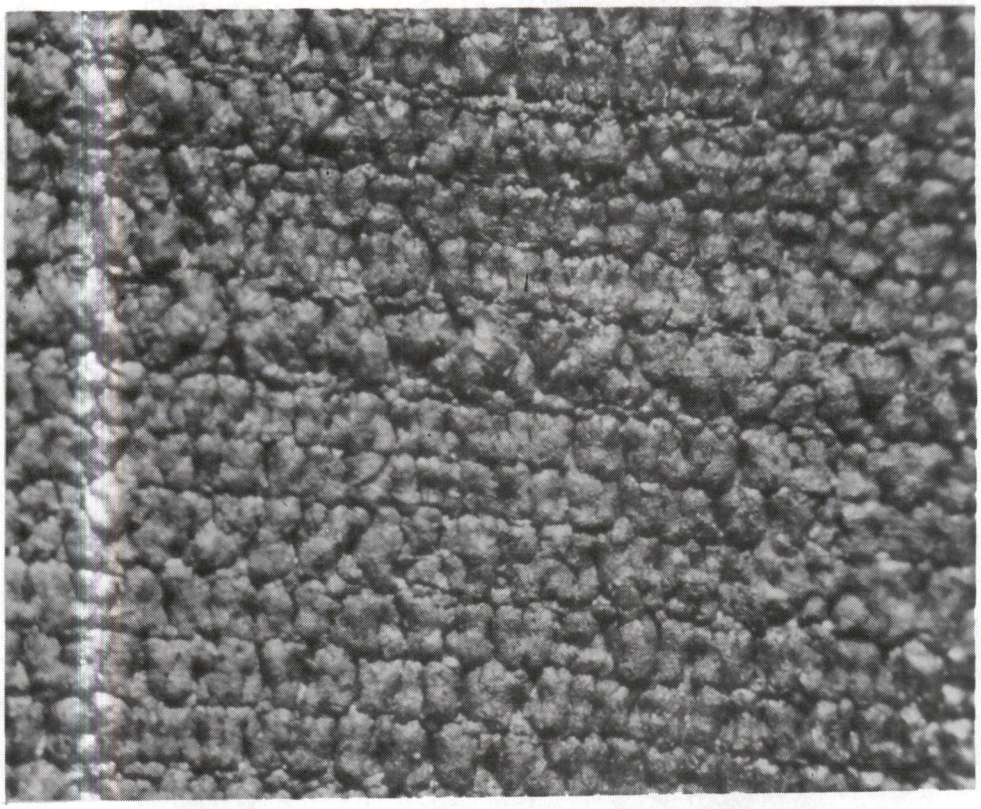

Figure 16. The surface of 2024 aluminum-boron thermally cycled in air, 12 minutes/cycle.

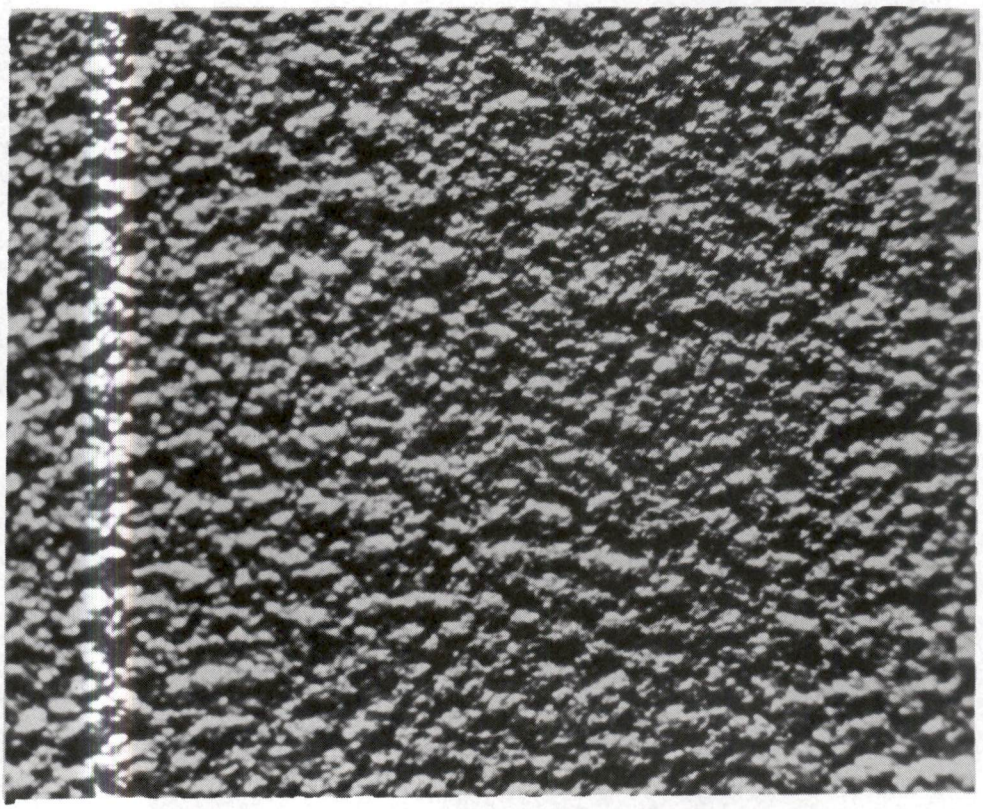

Figure 17. The surface of 1100 aluminum-boron thermally cycled in argon, 12 minutes/cycle.

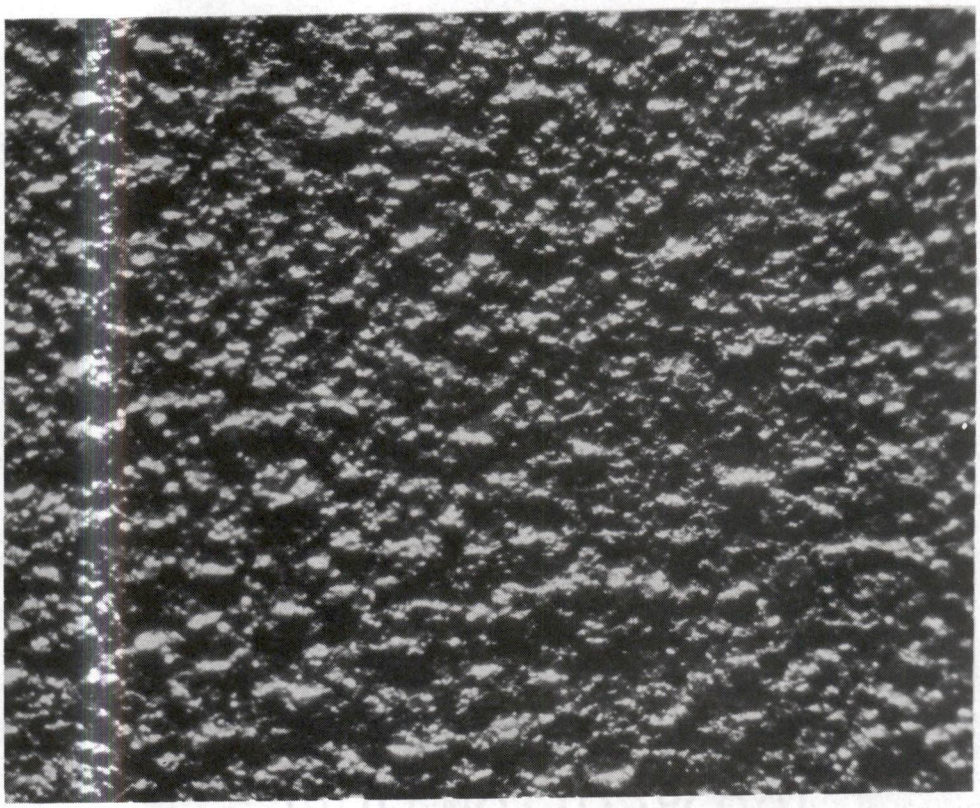

Figure 18. The surface of 1100 aluminum-boron thermally cycled in air, 12 minutes/cycle.

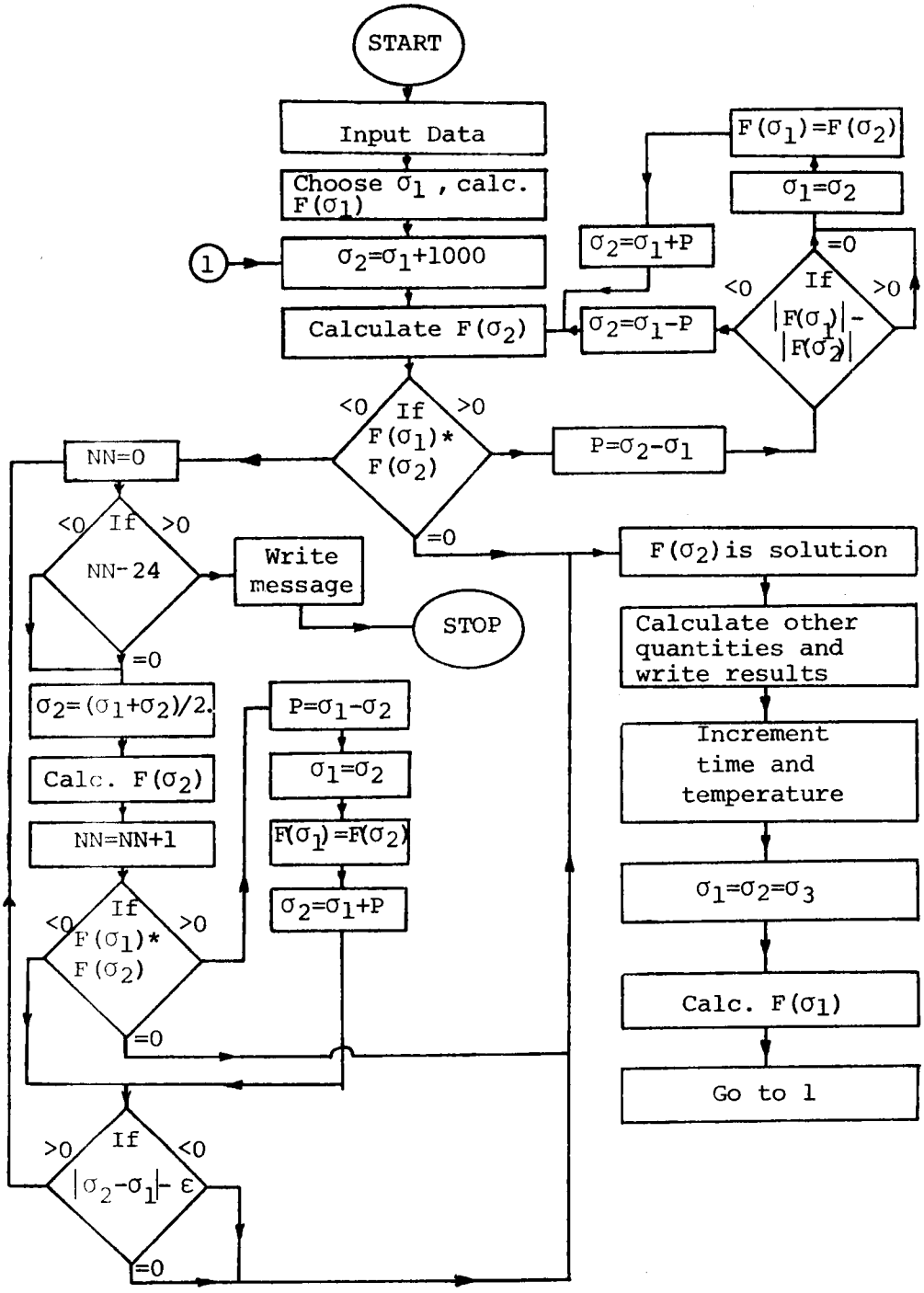

Figure 19. A flow-chart for the computation of composite thermal stresses and strains.

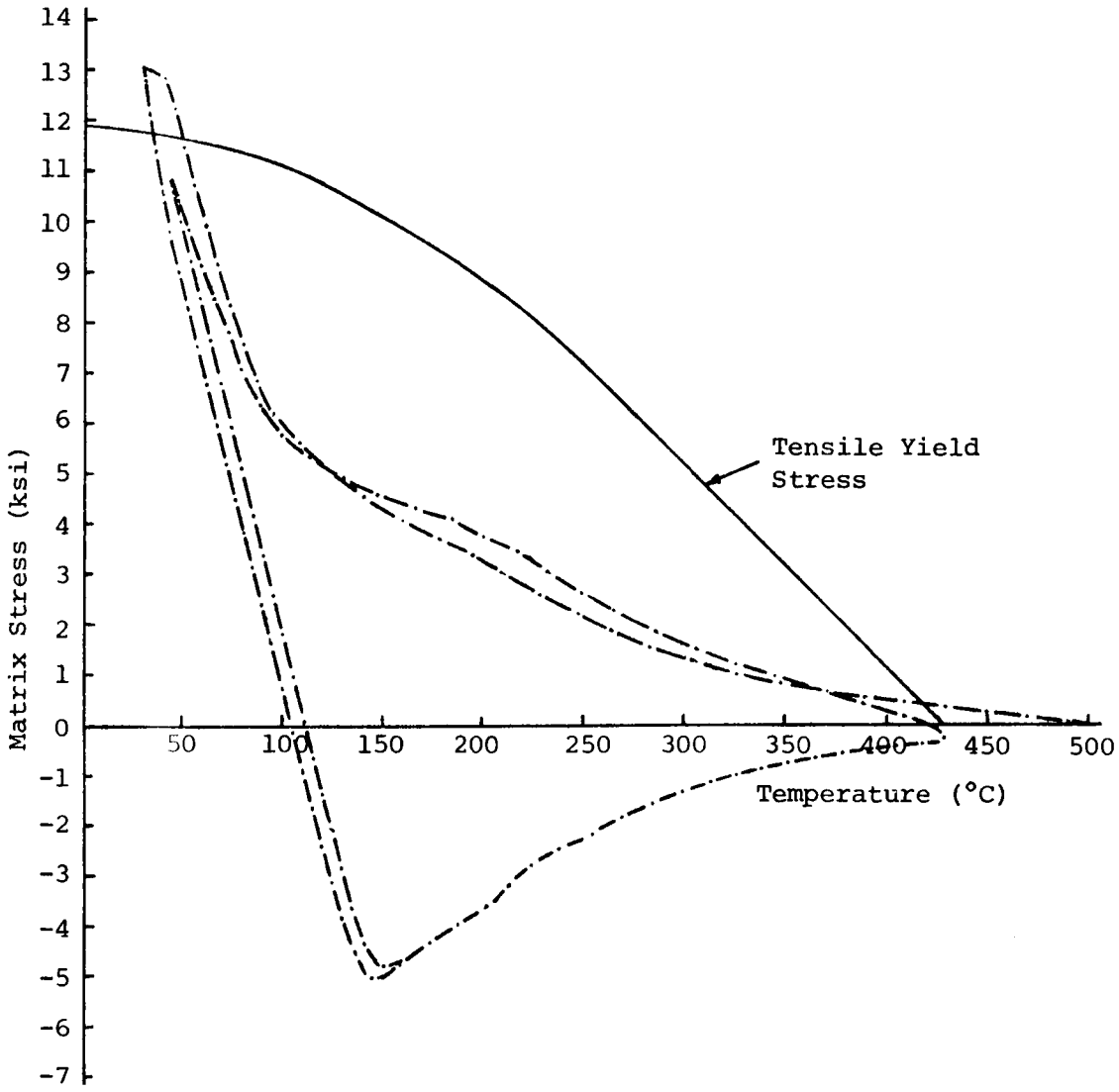

Figure 20. The matrix stress in thermally cycled 2024 aluminum-boron, 12 minutes/cycle.

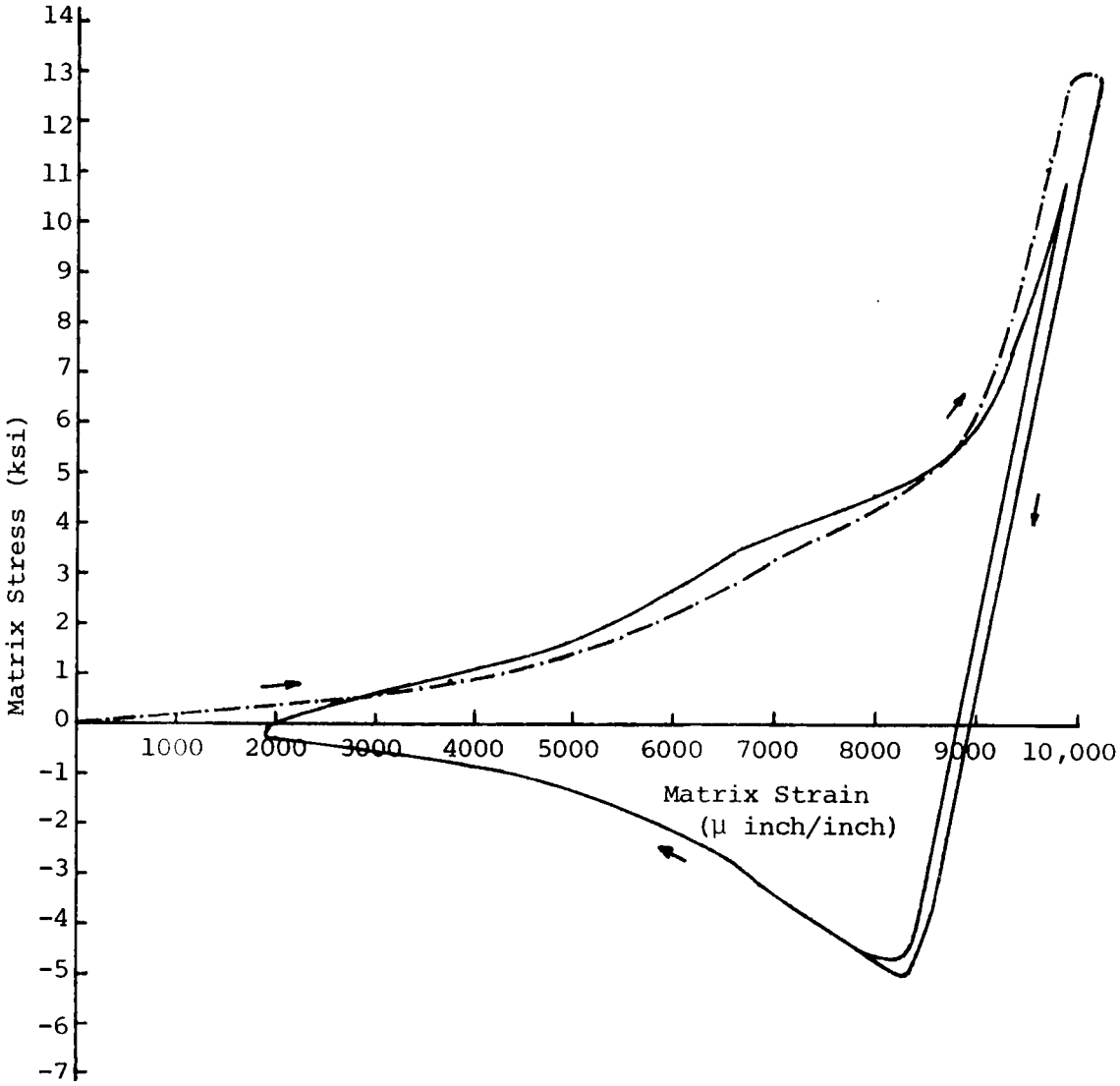

Figure 21. The matrix stress-strain curve during thermal cycling of 2024 aluminum-boron, 12 minutes/cycle.

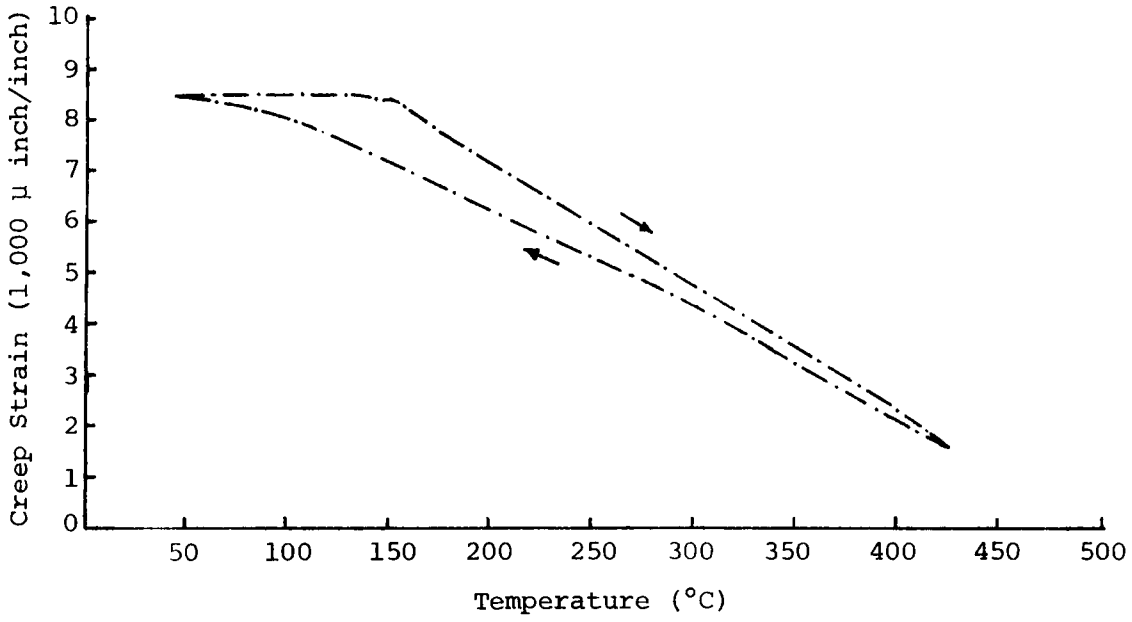

Figure 22. The creep strain during thermal cycling of 2024 aluminum-boron, 12 minutes/cycle.

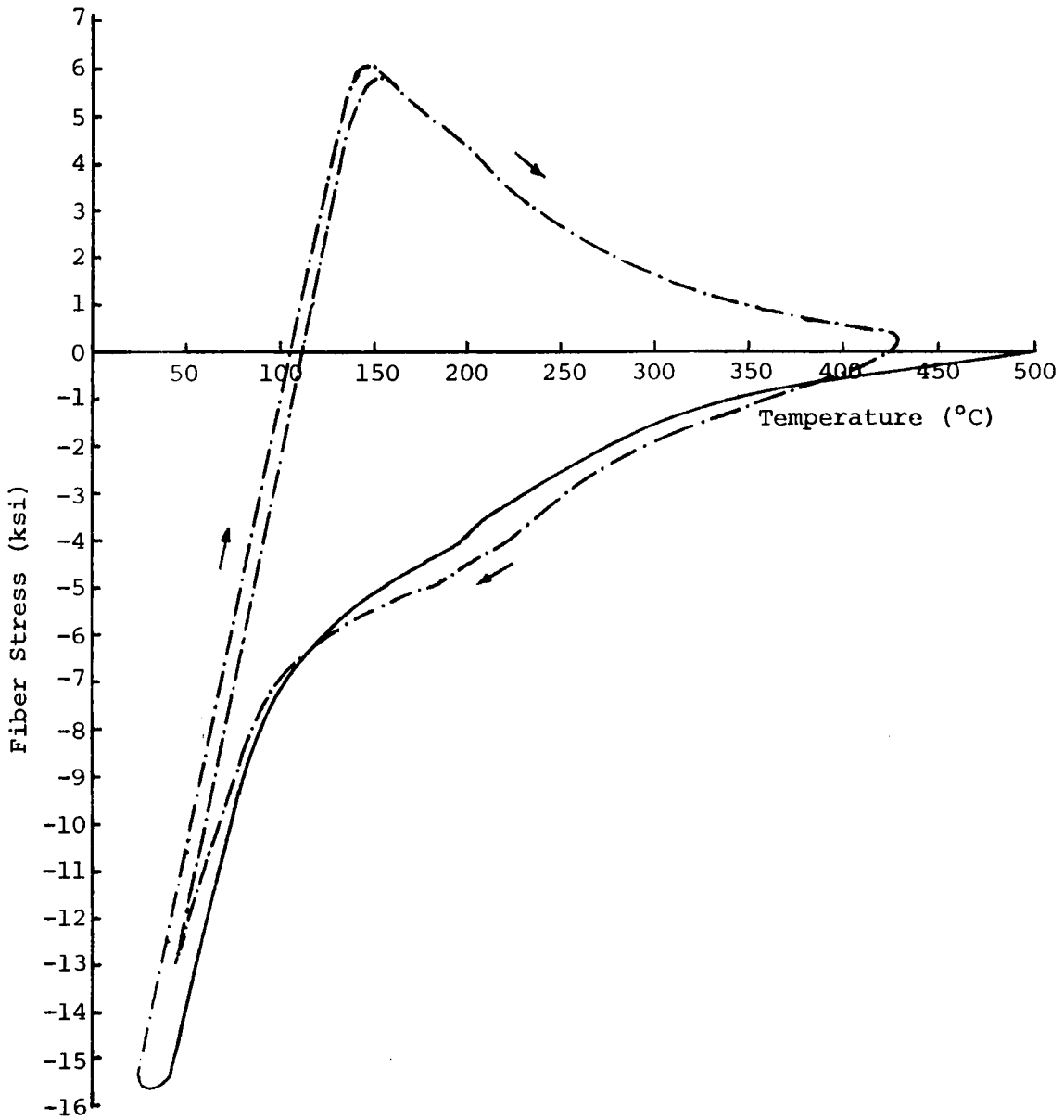

Figure 23. The fiber stress during thermal cycling of 2024 aluminum-boron, 12 minutes/cycle.

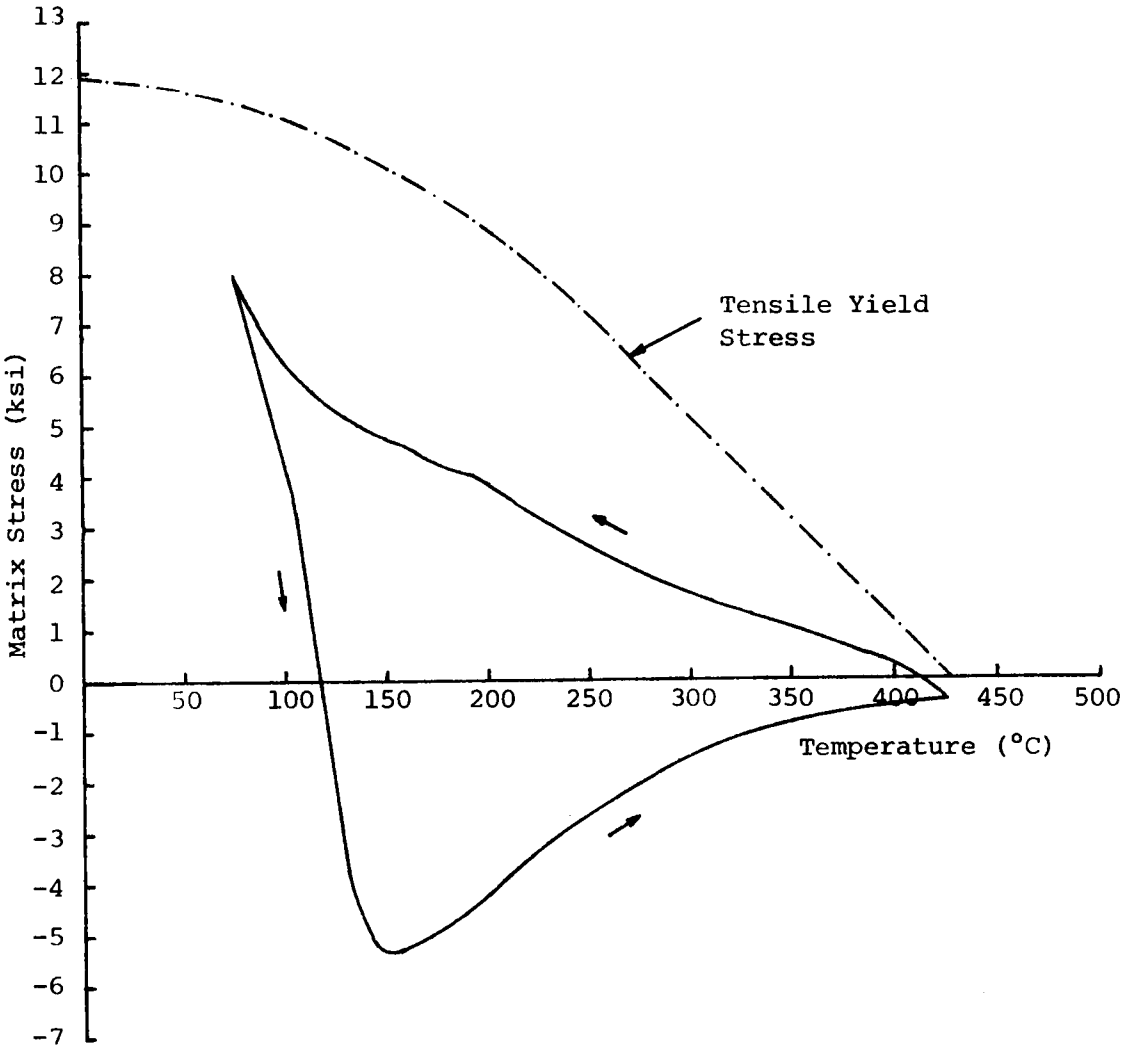

Figure 24. The matrix stress during thermal cycling of 2024 aluminum-boron, 6 minutes/cycle.

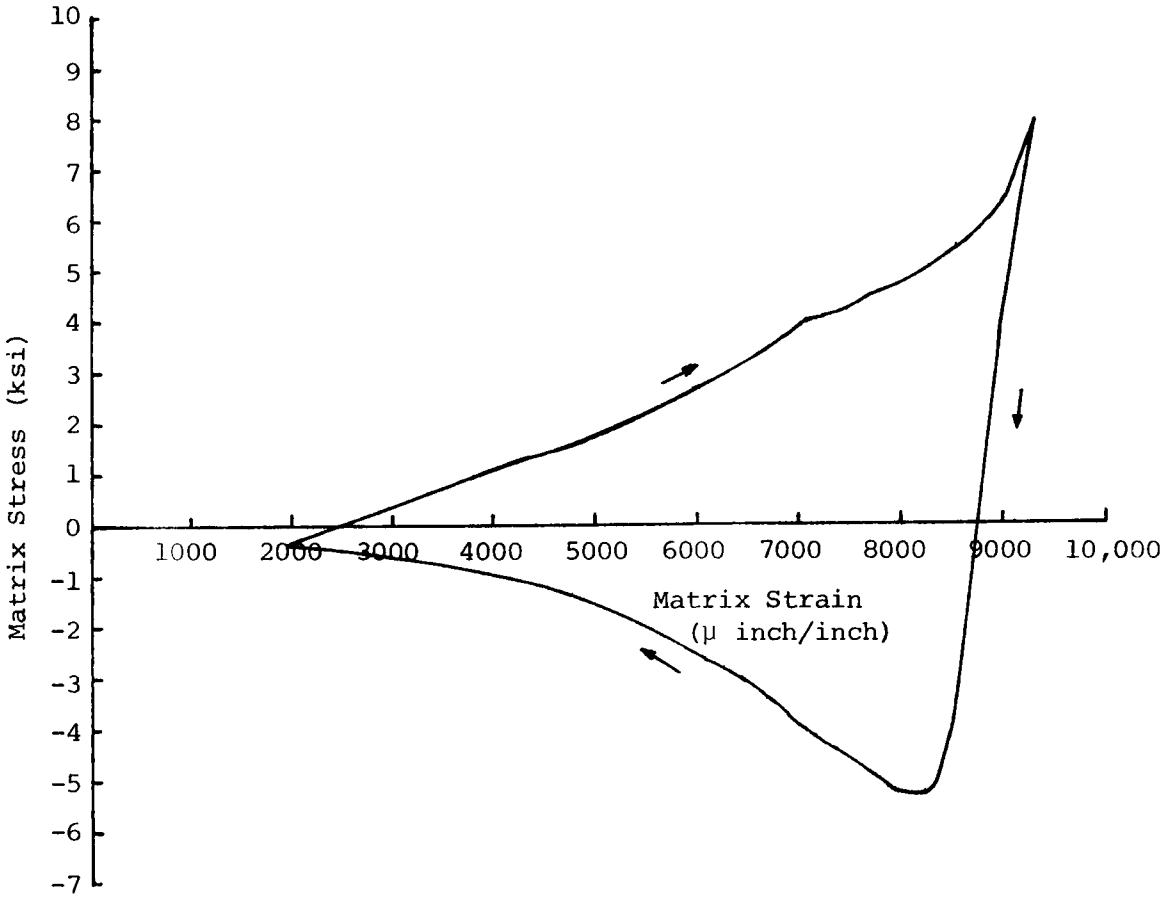

Figure 25. The matrix stress-strain curve during thermal cycling of 2024 aluminum-boron, 6 minutes/cycle.

VITA

Marvis Kelly White was born in Humphreys County, Tennessee, on July 15, 1950. He attended the public schools there and entered Tennessee Technological University in September, 1968. While attending Tennessee Technological University, he worked for two years as a co-operative student at the NASA Marshall Space Flight Center, Alabama. Immediately after receiving a Bachelor of Science degree in Engineering from Tennessee Technological University in August, 1973, he accepted a research assistantship at The University of Tennessee Space Institute. In August, 1976, he was awarded the Master of Science degree in Engineering Science.